Reviewed Preprint
v1 • May 28, 2026
Not revised

For correspondence:
Ulrich.Steidl@einsteinmed.edu
Robert.Coleman2@einsteinmed.edu

Competing interests: No competing interests declared

Funding: See page 24

Reviewing editor: Timothy J Stasevich, Colorado State University, United States

Transitory enhancement of GATA2 chromatin engagement during early erythroid differentiation

John W Hobbs[1,2], Samuel J Taylor[1,3], Rajni Kumari[1], Nayem Haque[1,2], Lou Lou Victor[1], Ulrich Steidl[1,4,5,6] ✉, Robert A Coleman[1,2,6] ✉

[1]Department of Cell Biology, Albert Einstein College of Medicine, Bronx, United States • [2]Gruss Lipper Biophotonics Center, Albert Einstein College of Medicine, Bronx, United States • [3]Department of Pediatrics Hematology & Oncology, WashU Medicine, St. Louis, United States • [4]Department of Oncology, Albert Einstein College of Medicine, Bronx, United States • [5]Ruth L. and David S. Gottesman Institute for Stem Cell Research and Regenerative Medicine, Albert Einstein College of Medicine, Bronx, United States • [6]Montefiore Einstein Comprehensive Cancer Center, Bronx, United States

eLife Assessment

This **important** study combines single-molecule imaging and CUT&TAG to address the molecular mechanism underlying the differentiation process that initiates the formation of red blood cells in the bone marrow. The authors provide evidence that the transcription factor GATA2 transiently associates with a new set of genomic loci early in the differentiation process before it is replaced by GATA1. Together, the experiments across three biological systems are **solid**, but they could benefit from additional details and controls to strengthen the conclusions.

https://doi.org/10.7554/eLife.111233.1.sa4

Abstract

Erythroid differentiation requires precise regulation of transcription factor binding to chromatin targets as hematopoietic progenitors relinquish multipotency and activate lineage programs. GATA2 maintains progenitor identity and is thought to be progressively silenced as GATA1 levels rise; however, the precise changes in GATA2 chromatin binding kinetics during this transition remain undefined. Here, we combined live-cell single-molecule imaging in cell lines and primary mouse progenitors with CUT&Tag chromatin profiling to define GATA2 activity during erythropoiesis. Single-molecule tracking resolved two interaction modes: short-lived (<1 s) searching interactions and long-lived (>5 s) binding. Surprisingly, early erythroid differentiation was characterized by a transitory strengthening of long-lived GATA2 chromatin engagement. This manifested as increased residence time of GATA2 bound to chromatin in G1E-ER4 cells and an expansion of the long-lived bound population in HPC7 cells and primary mouse progenitors. This transitory phase of enhanced engagement declined upon further differentiation. Genome-wide mapping identified regulatory elements selectively occupied by GATA2 during this early transition state, revealing promoter-proximal sites enriched for GATA/RUNX motifs and distal elements containing composite GATA/E-box signatures. Together, our imaging and chromatin profiling indicate that GATA2 chromatin engagement is kinetically remodeled at the onset of differentiation, with early recruitment targets partitioning into distinct promoter- and enhancer-associated subclasses. These results support a model in which transcription factor kinetics constitute a dynamic chromatin engagement layer that characterizes the GATA2-to-GATA1 transition.

Introduction

Cell-fate decisions during differentiation are orchestrated by transcription factors (TFs) that coordinate gene expression programs in a cell-type- and context-dependent manner (Lambert et al. 2018; Levine et al., 2014). In hematopoiesis, the commitment of multipotent progenitors requires transcriptional mechanisms that activate lineage-specific programs while restricting multipotency (Laurenti and Göttgens, 2018; Orkin and Zon, 2008). Hematopoietic TFs accomplish these functions by binding cis-regulatory elements and assembling complexes with cofactors that modulate transcriptional output (Heinz et al. 2015).

GATA2 is essential for maintaining hematopoietic stem and progenitor cell (HSPC) identity (Yamamoto et al. 1990; Katsumura and Bresnick 2017; de Pater et al. 2013). As a zinc-finger DNA-binding protein, GATA2 supports HSPC proliferation, survival, and the transcriptional programs that sustain progenitor potential (Tsai et al. 1994; Tsai and Orkin 1997). During erythropoiesis, *Gata2* expression decreases as *Gata1* expression increases. Although distinct in function, both factors recognize the WGATAR consensus motif. This property enables a regulatory transition in which the GATA2 protein promotes *Gata1* transcription with the GATA1 protein subsequently replacing GATA2 at shared genomic binding sites. This “GATA switch” is central to erythropoiesis (Johnson et al. 2020; Ross et al. 2012; Weiss et al. 1997). Disruption of this regulatory axis results in bone marrow failure, immune dysfunction, and a predisposition to MDS and AML (Homan et al. 2021; Spinner et al. 2014; Wlodarski, Collin, and Horwitz 2017).

Several model systems have been used to study GATA2 function during erythroid differentiation. The G1E-ER4 cell line represents an important model for dissecting the GATA1-induced regulatory switch (Weiss et al. 1997). G1E cells, derived from *Gata1*-null fetal liver, enable direct analysis of the GATA switch because re-expression of GATA1 induces terminal erythroid maturation via displacement of GATA2 from chromatin (Fujiwara et al. 2009; Suzuki et al. 2013). The widely used G1E-ER4 derivative cell line expresses a GATA1–estrogen receptor ligand binding domain fusion (GATA1-ER), allowing synchronized erythroid induction through controlled nuclear entry of GATA1. In contrast, Hematopoietic Progenitor Cell-7 (HPC7) cells maintain endogenous GATA2 and GATA1 regulation and represent a cytokine-responsive progenitor state in which GATA2 cooperates with factors such as FLI1, LMO2, SCL/TAL1, and RUNX1 to sustain multipotency (May et al. 2013; Tijssen et al. 2011). Mouse reporter models, including GATA2VENUS, have further defined *Gata2* expression dynamics in vivo (Ahmed et al. 2020). Although they have clarified many aspects of the GATA2-to-GATA1 transition, these systems rely primarily on static or population-level measurements, leaving the real-time dynamics of chromatin engagement unresolved.

Transcription factor interactions with chromatin are highly dynamic. Single-molecule imaging studies in mouse ES cells and cancer cell lines have shown that TFs alternate between brief chromatin interactions and multi-second long-lived engagements (Gebhardt et al. 2013; Liu et al. 2014; Morisaki et al. 2016). It is unknown how transcription factor chromatin binding kinetics change during differentiation. Specifically in hematopoiesis, researchers have not directly measured whether GATA2 chromatin engagement changes in magnitude or duration during the initiation of erythroid differentiation in live progenitors.

The necessity of resolving these dynamics at the single-cell level is underscored by recent studies revealing substantial heterogeneity and stochasticity in transcription states of hematopoietic cells. Single-molecule imaging of mRNA demonstrated that lineage-associated transcription factors, including *Gata1*, *Gata2*, and *Spi1*, are expressed at low copy number and frequently co-expressed within individual progenitor cells, despite appearing mutually exclusive in population-averaged or sequencing-based analyses (Wheat et al. 2020). Single-cell proteomic studies further showed that lineage commitment is accompanied by gradual, quantitative remodeling of transcription factor protein abundance rather than discrete binary switches (Palii et al. 2019). Together, these findings suggest that hematopoietic cell states are dynamic and probabilistic, and that transcription factor abundance alone may be insufficient to capture the regulatory mechanisms that govern lineage entry.

Here, we use a combination of single-molecule TF protein imaging and CUT&Tag chromatin profiling to define how GATA2 chromatin interaction modes and genomic occupancy change during erythroid differentiation. Together, these complementary approaches establish a dynamic framework revealing that erythroid entry is defined by a previously unappreciated distinct kinetic transition state.

Results

Single-molecule imaging reveals discrete kinetic modes of GATA2 chromatin binding in hematopoietic progenitor cells

To visualize GATA2 behavior at single-molecule resolution, we immobilized live hematopoietic progenitors on CD43-coated glass dishes (Loeffler et al. 2018) for highly inclined laminated optical sheet (HiLo) microscopy. We expressed GATA2 as a HaloTag (Los et al. 2008) fusion (GATA2–Halo) containing a destabilization domain, allowing temporal control of protein levels via ligand-dependent stabilization. Upon addition of Shield-1, the fusion protein was stabilized and labeled with limiting Janelia Fluor-646 HaloTag ligand to achieve the sparse density required for single-molecule tracking. Shield-1–dependent accumulation of GATA2-Halo was confirmed in live HPC7 cells (Figure 1A; Supplementary Video 1)

Single-molecule time-lapse imaging with a 500 ms exposure blurred out freely diffusing molecules, leaving only chromatin-bound GATA2–Halo visible as distinct fluorescent spots (Figure 1B; Supplementary Video 2). Trajectories were reconstructed and analyzed using the STRAP pipeline (Haque and Coleman 2025). The resulting dwell-time distribution was best fit by a double-exponential model, resolving short-lived (<1 s, ~80%) and long-lived (>5 s, ~20%) binding GATA2-Halo molecules (Figure 1C). Consistent with established single-molecule frameworks (Gebhardt et al. 2013; Liu et al. 2014), we attribute the short-lived population to non-specific chromatin scanning (Figure 1D, left) and the long-lived population to stable, sequence-specific regulatory engagement (Figure 1D, right).

Our data analysis pipeline provides several metrics related to chromatin-binding kinetics at the single-cell level, including (i) the total number of binding events, (ii) the proportion of molecules in the long-lived binding population (>5 s), and (iii) long-lived residence-time distributions. Plotting these metrics across a population of basal progenitor cells revealed substantial cell-to-cell heterogeneity of GATA2–Halo chromatin binding (Figure 1E). This heterogeneity suggests that individual cells within an otherwise defined progenitor population exhibit markedly different levels of GATA2 engagement with chromatin. For subsequent cell-state comparisons, we therefore focused primarily on the long-lived binding fraction, which reflects chromatin engagement associated with regulatory function (Figure 1D). Short-lived (<1 s) binding events were quantified separately and are reported in Figure Supplement 1.

Transitory enhancement of GATA2 chromatin engagement during early erythroid differentiation in G1E-ER4 cells

The G1E-ER4 cell line provides a well-established model for synchronized erythroid differentiation through inducible nuclear entry of GATA1 (Weiss et al. 1997; Fujiwara et al. 2009; Suzuki et al. 2013). In this system, treatment with 4-hydroxytamoxifen (4-OHT) drives nuclear entry of GATA1–ER, initiating erythroid differentiation. Single-molecule imaging was performed in cells undergoing Basal progenitor (0 h**)**, Early erythroid (2 h), and Late erythroid (24 h) states (Figure 2A; Supplementary Video 2). We confirmed expected erythroid progression using orthogonal protein and chromatin-based assays (Figure Supplement 2A-C). Western blot analysis showed progressive accumulation of GATA1 protein across the time course, while genome-wide CUT&Tag profiling revealed reciprocal changes in GATA factor occupancy at canonical erythroid regulatory loci, including *Kit*, *Gata2*, and *Klf1*. At these GATA-switch genes, GATA2 occupancy decreased while GATA1 binding increased during differentiation, consistent with prior studies (Suzuki et al. 2013) and validating our staging.

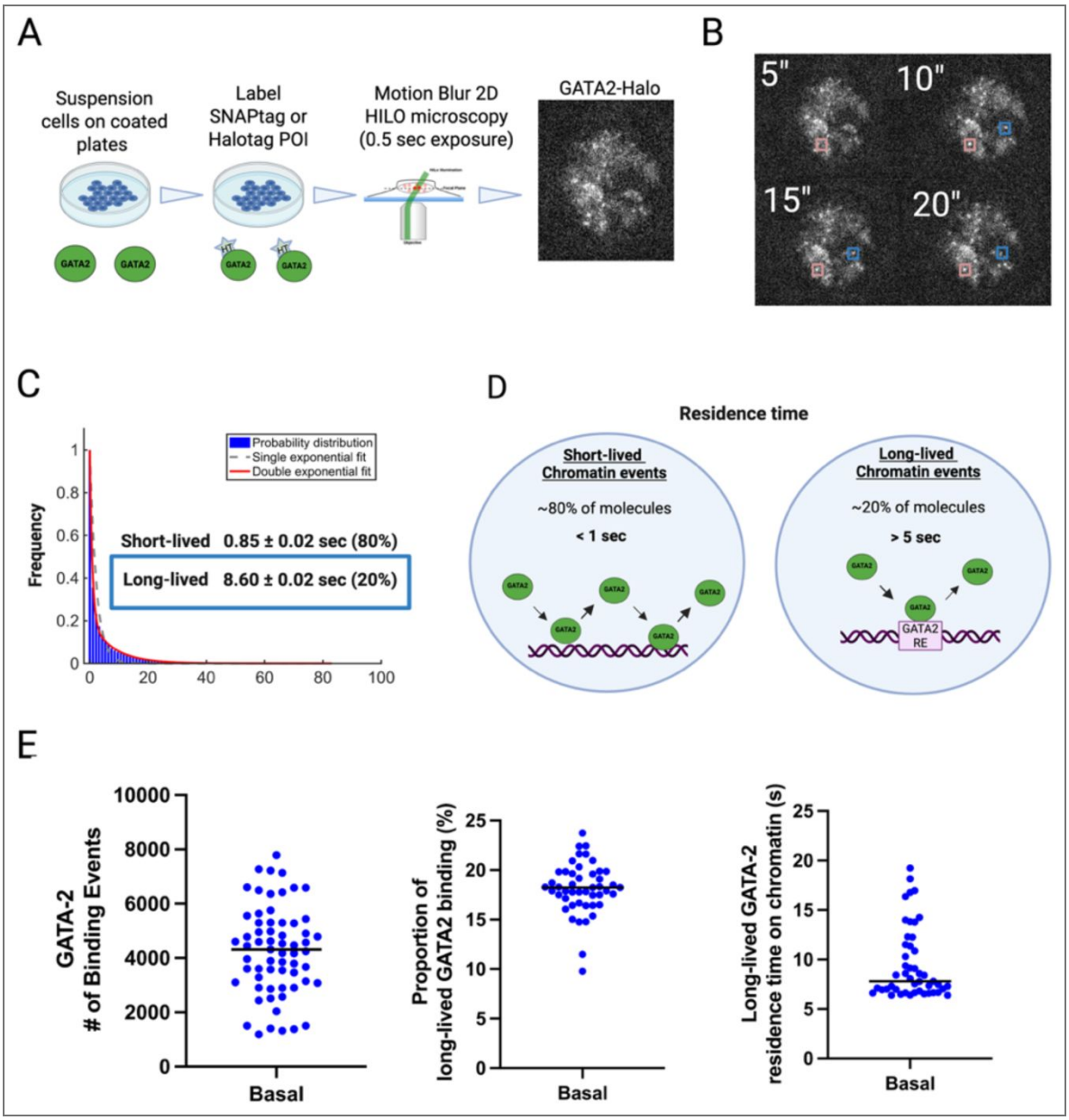

Figure 1. Single-molecule imaging reveals discrete GATA2 kinetic modes in hematopoietic progenitor cells.

(A) Schematic of the live-cell single-molecule imaging workflow. Suspension cells were secured to the surface of an imaging dish using CD43-mediated immobilization and imaged by HiLo microscopy using 500-ms exposure times to preferentially detect chromatin-bound GATA2 molecules with multi-second residence times. **(B)** Representative time-lapse sequences illustrating two measurable GATA2 interaction modes. Short-lived interactions (<1 s) appear as brief sampling contacts in which GATA2 rapidly binds and unbinds chromatin. Long-lived interactions (>5 s) correspond to multi-second chromatin-bound events in which GATA2 remains localized at a single site. **(C)** Residence time distribution of GATA2 trajectories from a single representative cell fit with a double-exponential model, resolving a short-lived kinetic component (<1 s) and a long-lived component (>5 s) corresponding to chromatin engagement. **(D)** Schematic depiction of the interaction framework used throughout this study. Left: short-lived target-search behavior, in which GATA2 rapidly engages and disengages chromatin during chromatin scanning. Right: long-lived chromatin engagement, in which GATA2 remains localized at a defined regulatory element (RE) for several seconds. **(E)** Quantification of baseline kinetic parameters in **Basal progenitor cells (0 h)**, including total binding events per cell, fraction of molecules in the long-lived binding population (>5 s), and per-cell dwell-time distributions. Each point represents a single cell (N = 47), revealing substantial cell-to-cell heterogeneity in GATA2–Halo chromatin binding. Created using *BioRender.com*.

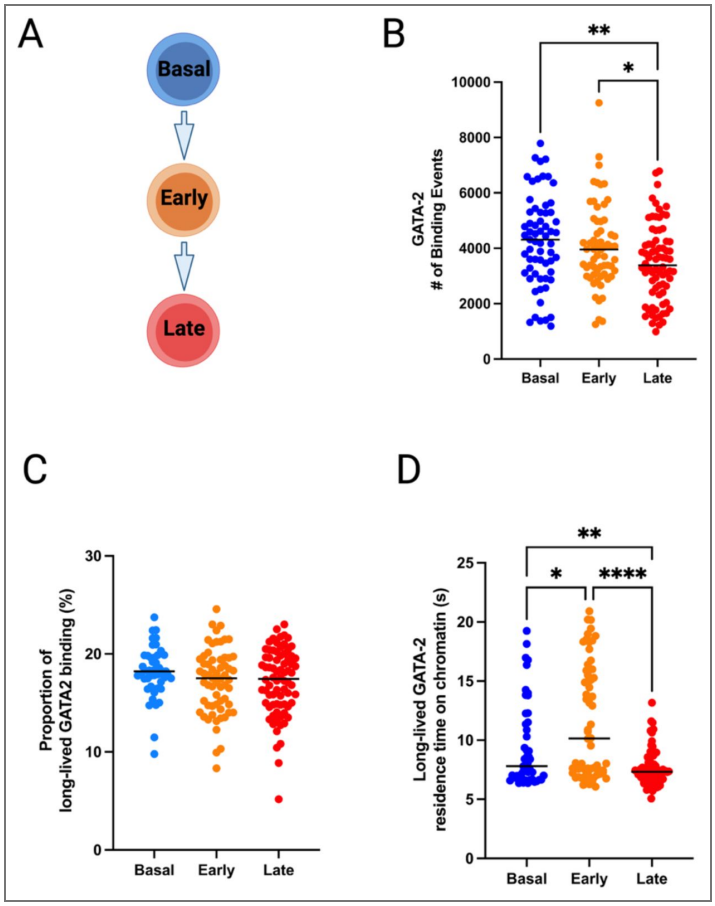

Figure 2. GATA2 binding dynamics exhibit a transitory strengthening of long-lived chromatin engagement during Early erythroid differentiation in G1E-ER4 cells.

(A) Schematic of the G1E-ER4 differentiation system. Activation of GATA1–ER with 4-hydroxytamoxifen induces progression from the Basal progenitor (0 h) to Early erythroid (2 h) and Late erythroid (24 h) states. **(B)** Total number of detectable GATA2 chromatin binding events per cell across erythroid stages. Binding-event frequency is unchanged between Basal and Early states but is reduced in the Late state relative to both Basal and Early erythroid cells. **(C)** Fraction of GATA2 molecules engaging in long-lived chromatin interactions across erythroid stages. The proportion of long-lived binding events remains constant across Basal, Early, and Late states (approximately 20%). **(D)** Residence times of long-lived GATA2 chromatin interactions across erythroid stages. Residence time is significantly prolonged in the Early erythroid state relative to the Basal progenitor state and is significantly reduced in the Late erythroid state. Each point represents a single cell (Basal, N = 47; Early, N = 62; Late, N = 76). Bars indicate mean ± SEM. Statistical significance was assessed using the Brown–Forsythe and Welch ANOVA with Games–Howell post hoc correction. Significance levels are indicated as follows: * $P < 0.05$; ** $P < 0.01$; **** $P < 0.0001$. Created using *BioRender.com*.

Single-molecule imaging showed that the total number of detectable GATA2 chromatin binding events per cell was unchanged between Basal progenitor and Early erythroid states. In contrast, GATA2 chromatin binding declined by approximately 19% in the Late erythroid state relative to Basal and by approximately 15% relative to the Early state (Figure 2B). Because exogenous GATA2–Halo expression was externally stabilized during imaging, the reduction in detectable binding events in Late erythroid cells likely reflects changes in GATA2's ability to engage chromatin rather than differences in protein levels. Despite this reduction, the fraction of molecules in the long-lived chromatin binding population remained constant across all stages at approximately 20% (Figure 2C). Early erythroid cells exhibited a significant increase in the chromatin binding residence time of the long-lived binding population relative to Basal progenitors (mean 11.58 vs. 9.54 s; ~21% increase; $p = 0.034$). In contrast, residence times declined significantly in Late erythroid cells (mean 7.58 s), representing a ~21% decrease relative to Basal progenitors ($p = 0.0023$) and a ~35% decrease relative to Early erythroid cells ($p < 0.0001$) (Figure 2D).

Together, these data identify Early erythroid transition as a distinct and transitory kinetic state, characterized by a specific enhancement of GATA2 chromatin engagement dynamics that is not observed in either Basal progenitors or Late erythroid cells. This transitory enhancement occurs at the level of chromatin binding residence time, without expansion of the long-lived binding molecule population. This indicates that Early erythroid entry is marked by changes in chromatin binding behavior rather than increased occupancy. Loss of this kinetic signature in Late erythroid cells is consistent with the established attenuation of GATA2 activity during erythroid commitment, placing this effect within a narrow temporal window of differentiation during which GATA2 chromatin engagement dynamics are transiently enhanced.

Dynamic regulation of GATA2 chromatin engagement during cytokine mediated HPC7 differentiation

While G1E-ER4 cells have served as a gold-standard model for interrogating the GATA1-induced GATA switch, this system relies on enforced nuclear entry of GATA1 and therefore represents a highly engineered differentiation paradigm. We next asked whether the early strengthening of GATA2 chromatin engagement observed in G1E-ER4 cells also occurs under cytokine-driven differentiation conditions. To address this, we applied a similar single-molecule imaging strategy in HPC7 cells, a hematopoietic progenitor line in which endogenous GATA2 and GATA1 regulation is preserved, and erythroid differentiation is induced by erythropoietin (EPO) stimulation (Supplementary Video 3) (May et al. 2013; Sasca et al. 2019). This approach provides a complementary system in which erythroid entry is initiated by extracellular signaling rather than enforced nuclear localization of GATA1.

Single-molecule imaging in HPC7 cells revealed a pronounced increase in GATA2 chromatin binding events upon cytokine-driven differentiation. The total number of detectable GATA2 chromatin binding events per cell increased significantly from the Basal state to the Early erythroid stage following EPO stimulation and remained elevated in the Late stage (Figure 3B). While the chromatin binding event frequency was markedly higher in both Early and Late erythroid cells compared with Basal progenitors ($p < 0.0001$), no significant difference was observed between Early and Late stages. To assess functional GATA2 chromatin engagement during cytokine-driven differentiation in HPC7 cells, we quantified the fraction of GATA2 molecules engaged in long-lived chromatin binding events across Basal, Early, and Late erythroid stages. In Basal cells, a mean of approximately 2.6% of total GATA2 binding events were classified as long-lived (>5 s). This long-lived chromatin binding fraction increased significantly during the Early erythroid stage, reaching a mean of 4.4% ($p = 0.0067$), before declining in Late erythroid cells to levels comparable to Basal (~2.0%; $p = 0.51$) (Figure 3C). Notably, Early erythroid cells exhibited a pronounced skew toward higher long-lived chromatin binding fractions at the single-cell level compared with both Basal and Late states. Together, these data indicate that a subset of Early erythroid cells acquires an enhanced capacity for long-lived GATA2 chromatin engagement.

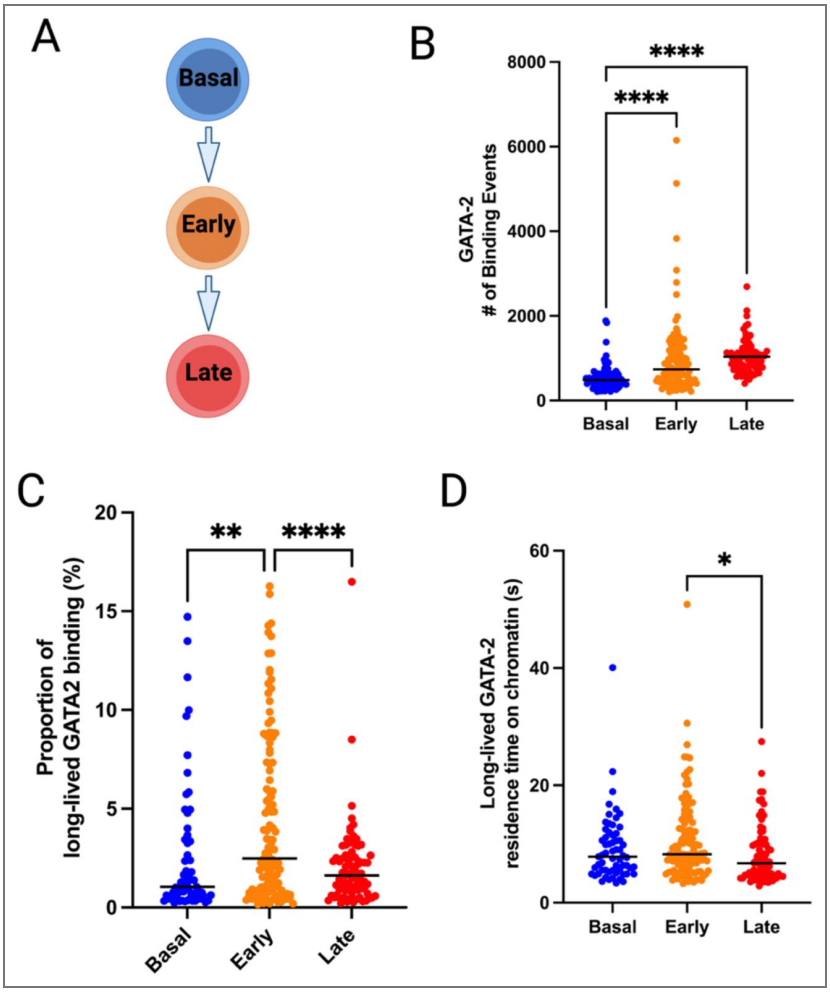

Figure 3. Early erythroid entry in HPC7 progenitors is marked by a transitory increase in long-lived GATA2 chromatin engagement.

(A) Schematic of the HPC7 erythroid differentiation paradigm. Erythropoietin (EPO) stimulation induces progression from the Basal progenitor state to Early and Late erythroid stages. **(B)** Total number of detectable GATA2 chromatin binding events per cell across erythroid stages. Binding-event frequency increases significantly from the Basal to Early stage following EPO stimulation and remains elevated in the Late stage, with no significant difference between Early and Late populations. **(C)** Fraction of GATA2 molecules engaging in long-lived chromatin interactions across erythroid stages. The long-lived binding fraction is significantly increased in Early erythroid cells relative to Basal progenitors and declines in Late erythroid cells to levels comparable to Basal. **(D)** Residence times of long-lived GATA2 chromatin interactions across erythroid stages. Residence times are similar between Basal and Early stages and are modestly reduced in Late erythroid cells relative to the Early stage. Each point represents a single cell. Bars indicate mean ± SEM. Statistical significance was assessed using the Brown–Forsythe and Welch ANOVA with Games–Howell post hoc correction. Statistical significance was defined as $P < 0.05$. Significance levels are indicated as follows: * $P < 0.05$; ** $P < 0.01$; *** $P < 0.001$; **** $P < 0.0001$. Created using *BioRender.com*.

We next examined GATA2 chromatin residence times across Basal, Early, and Late erythroid stages in HPC7 cells. The residence time of long-lived GATA2 chromatin interactions was not significantly altered during the Early erythroid transition but was modestly reduced in Late erythroid cells relative to the preceding stage (Figure 3D). This indicates that, in contrast to the Early expansion of the long-lived binding population, changes in GATA2 residence time in HPC7 cells primarily emerge upon the Late stage of erythroid commitment rather than during the initial priming phase.

Short-lived (<1 s) GATA2 interactions were also quantified (Figure Supplement 1C, D). Consistent with the expansion of the long-lived chromatin binding population, the proportion of short-lived binding events decreased in Early erythroid cells. Within the temporal resolution of our measurements, we additionally observed a subtle but significant reduction in the mean residence times of short-lived binding events in Late erythroid cells. Together, these data indicate that the primary characteristics of GATA2 dynamics in HPC7 cells are defined by (i) an Early expansion of the long-lived chromatin binding population during erythroid priming and (ii) a subsequent loss of GATA2 engagement accompanied by reduced residence times of short-lived binding events in the Late stage of erythroid commitment.

These findings indicate that HPC7 progenitors undergo a two-step kinetic transition, characterized by an early expansion of the long-lived binding population during erythroid priming, followed by loss of long-lived GATA2 engagement and reduced residence times upon commitment. Taken together, both examined cell line differentiation models G1E-ER4 and HPC7 converge on a shared principle in which Early erythroid entry represents a transitory kinetic state of enhanced chromatin engagement.

GATA2 chromatin engagement is transiently enriched in Early erythroid progenitors in vivo

To evaluate GATA2 dynamics under physiological in vivo conditions, we generated a transgenic mouse model in which a SNAP-tag was inserted in frame at the 3' end of the endogenous *Gata2* coding sequence (GATA2–SNAP; Figure 4A). Prior transgenic mouse models expressing C-terminally tagged GATA2 proteins indicated minimal perturbation of GATA2 function (Ahmed et al., 2020). Accordingly, our SNAP-tagging strategy was designed to preserve endogenous GATA2 expression and regulatory control during hematopoiesis. Consistent with this, the knock-in allele supported normal viability and fertility and did not produce overt hematopoietic abnormalities under the conditions examined, indicating that measurements were obtained in a physiologically competent background.

To define changes in GATA2 chromatin binding dynamics during in vivo erythropoiesis, we isolated primary cells from GATA2–SNAP homozygous mice by flow cytometry to resolve Basal, Early, and Late erythroid populations (Figure 4A). Live-cell single-molecule imaging was performed on these flow-sorted populations by labeling GATA2–SNAP with limiting concentrations of SNAP-Cell 647-SiR SNAP-tag ligand to achieve sparse single-molecule detection, analogous to the HaloTag-based imaging strategy used in the cell line models (Supplementary Video 4). The number of detectable chromatin binding events of endogenously expressed GATA2 increased markedly in Early erythroid cells compared with the Basal population (mean 751.9 vs. 432.3 binding events per cell; ~74% increase; Figure 4B). In contrast, Late erythroid cells exhibited a substantial reduction in GATA2 chromatin binding events relative to both Basal (mean 276.3; ~36% decrease) and Early populations (~63% decrease). This resulted in a three-tier distribution in which Early cells displayed the highest GATA2 chromatin binding event frequency, Basal cells were intermediate, and Late cells showed the lowest levels of chromatin binding (Figure 4B; all pairwise comparisons $p < 0.0001$). This increase in chromatin binding events in Early erythroid cells may reflect elevated GATA2 protein levels or, alternatively, an increased fraction of GATA2 molecules capable of engaging chromatin.

We therefore quantified the fraction of GATA2 molecules engaging in long-lived chromatin interactions across Basal, Early, and Late erythroid populations. In Basal cells, a mean of approximately 1.2% of GATA2 binding events resulted in long-lived chromatin engagement,

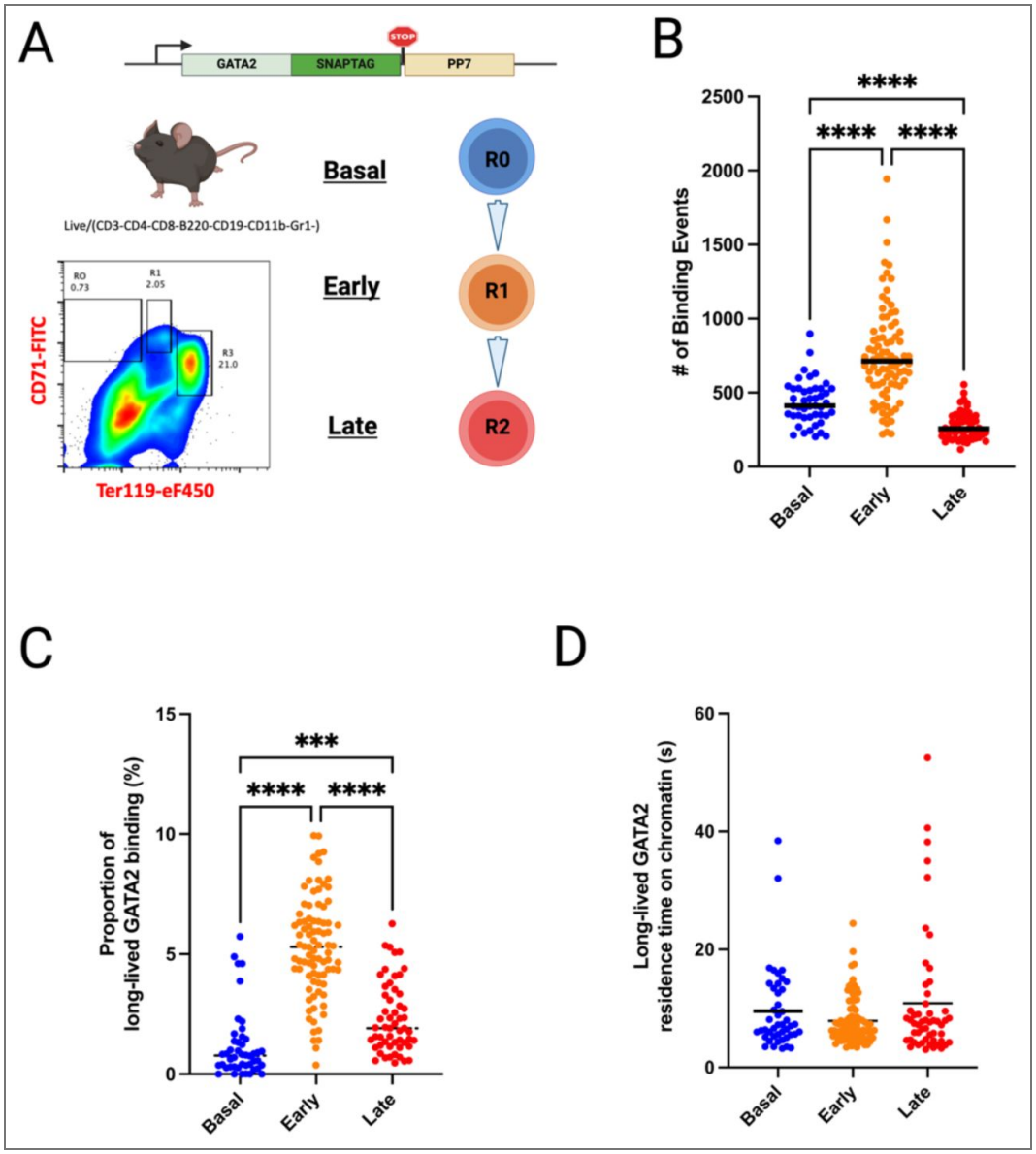

Figure 4. Endogenous GATA2 exhibits transitory enrichment of long-lived chromatin interactions during in vivo erythroid maturation.

(A) Schematic of the *Gata2*–SNAP knock-in mouse used for endogenous single-molecule imaging, together with the CD71/Ter119 flow-cytometry gating strategy used to define Basal, Early, and Late erythroid populations. **(B)** Total detectable GATA2 chromatin binding events per cell across Basal, Early, and Late erythroid populations. Binding-event frequency is highest in Early cells and reduced in Late cells. **(C)** Fraction of GATA2 molecules engaging in long-lived chromatin interactions across Basal, Early, and Late erythroid populations. The long-lived binding fraction is highest in Early cells and declines upon progression to the Late stage. **(D)** Residence times of long-lived GATA2 chromatin interactions across erythroid stages. Residence times are similar across all three populations, indicating that regulation primarily occurs through changes in the occupancy of the long-lived binding state rather than binding duration. Each point represents a single cell. Bars indicate mean ± SEM. Statistical significance was evaluated using the Brown–Forsythe and Welch ANOVA test with Games–Howell post hoc correction. Statistical significance was defined as $P < 0.05$. Significance levels are indicated as follows: * $P < 0.05$; ** $P < 0.01$; *** $P < 0.001$; **** $P < 0.0001$. Created using *BioRender.com*.

whereas this fraction increased markedly to approximately 5.3% in Early erythroid cells (Figure 4C). The fraction of long-lived GATA2 chromatin binding events declined to an intermediate level of approximately 2.3% in Late cells, which remained significantly higher than Basal cells but substantially lower than Early erythroid cells (Figure 4C). These data indicate that Early erythroid cells exhibit a pronounced enhancement in long-lived GATA2 chromatin engagement driven by an expansion of the long-lived binding population, which is partially attenuated as cells progress to the Late stage.

To further define the properties of long-lived chromatin-bound GATA2 molecules, we examined the residence times of long-lived binding events across Basal, Early, and Late erythroid populations. Residence times were similar across all three stages, with no significant differences detected between populations (Figure 4D). Notably, a small subset of multi-second binding events persisted in Late erythroid cells, consistent with continued retention of a limited set of regulatory interactions as transcriptional programs consolidate.

In contrast, short-lived (<1 s) GATA2 interactions exhibited pronounced stage-dependent differences. Residence times increased significantly in Early erythroid cells relative to Basal cells (mean 0.73 s vs. 0.55 s; $p < 0.0001$) and declined in Late cells (mean 0.58 s), while remaining significantly higher than Basal levels (Figure Supplement 1E–F). Together, these results indicate that long-lived GATA2 engagement is regulated primarily at the level of occupancy of the long-lived binding state rather than its residence time. By contrast, Early erythroid differentiation is accompanied by a slowing of GATA2 target-search dynamics within the short-lived binding population, an effect that is partially reversed later during erythroid differentiation.

In summary, single-molecule measurements in primary cells further support a model in which endogenous GATA2 exhibits a transitory enhancement of long-lived chromatin engagement during Early erythroid differentiation, consistent with the pattern observed in HPC7 cells. While the specific kinetic manifestation slightly differs in the different models, all studied systems including cell lines models and primary cells reveal a conserved Early erythroid window in which GATA2 chromatin engagement is transiently strengthened before it is subsequently attenuated at a later stage of erythroid differentiation.

Early erythroid–restricted GATA2 peaks resolve promoter-proximal and enhancer-associated regulatory subclasses

Across all systems examined, entry into the early erythroid state is associated with a transitory strengthening of GATA2 chromatin engagement. Leveraging the high degree of synchronization in the G1E-ER4 system to capture this transitory window, we profiled genome-wide GATA2 binding using CUT&Tag to determine whether this kinetic transition is accompanied by specific changes in genomic occupancy. Importantly, chromatin occupancy was mapped using an antibody targeting the HaloTag, leveraging the unique epitope to ensure that detected peaks reflect specific binding of the functional GATA2 fusion protein. Using a consensus peak universe approach, we identified 5,962 GATA2-occupied regions in Basal progenitors, 5,175 in Early erythroid cells, and 4,749 in Late erythroid cells (Figure 5A). Genome-wide CUT&Tag signal heatmaps across each category confirmed stage-restricted enrichment and validated our new temporal classification (Figure Supplement 3).

Given the enhanced chromatin engagement observed with live-cell single-molecule imaging in Early erythroid cells, we next focused on isolating genomic regions uniquely occupied during this window. Early erythroid–restricted sites were defined as peaks present exclusively at the Early stage and absent at both Basal and Late stages, yielding 1,167 Early erythroid–restricted peaks (Figure 5B). By requiring complete absence outside the Early erythroid state, this definition yields a narrower, high-confidence peak set that parallels the enhanced chromatin engagement observedin live-cell single-molecule imaging, offering greater specificity than the broader categories identified by intersection analysis.

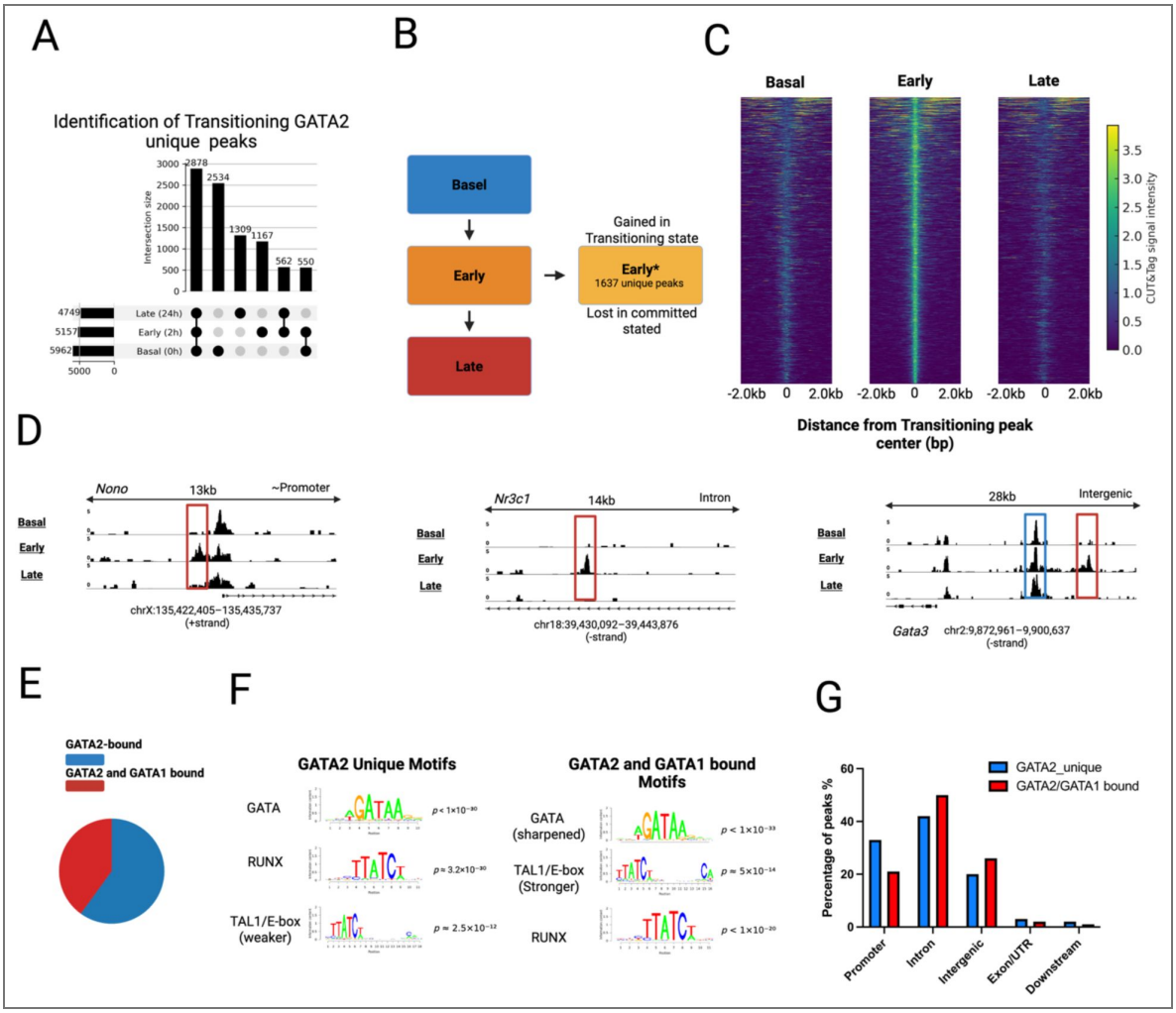

Figure 5. Early erythroid–restricted GATA2 peaks reveal temporally specific recruitment, two regulatory subclasses, and distinct motif and genomic features.

(A) Categorical classification of GATA2 CUT&Tag peaks across Basal progenitor (0 h), Early erythroid (2 h), and Late erythroid (24 h) G1E-ER4 cells. Peaks were grouped into Early-enriched, shared, Late-acquired, and monotonic categories, providing a global view of how GATA2 genomic occupancy evolves during erythroid differentiation. **(B)** Identification of Early erythroid–restricted GATA2 peaks. A stringent subset of peaks was defined as sites detected by MACS2 exclusively at the Early (2 h) erythroid state ($q < 0.01$) and absent at both Basal (0 h) and Late (24 h) stages using identical processing parameters. These peaks represent genomic regions uniquely recruited during Early erythroid entry. **(C)** CUT&Tag signal heatmap for all Early erythroid–restricted GATA2 peaks (n = 1,167) aligned to peak centers (±2 kb). Peaks show strong, centered GATA2 enrichment at the Early (2 h) stage with minimal signal at Basal (0 h) and Late (24 h) stages, indicating stage-specific recruitment. **(D)** Genome browser views of representative Early erythroid–restricted GATA2 peaks (highlighted by red boxes), including a promoter-proximal peak near *Nono*, an intronic site within *Nr3c1*, and an intergenic site near *Gata3*. Each locus exhibits GATA2 binding selectively in the Early erythroid state and loss in the Late erythroid state. Blue boxes indicate adjacent genomic regions lacking stage-dependent changes in GATA2 signal. **(E)** Classification of Early erythroid–restricted peaks based on overlap with GATA1 CUT&Tag data. Peaks were subdivided into GATA2-only peaks (n = 700) and peaks bound by both GATA2 and GATA1 (n = 467), indicating that Early GATA2 recruitment can occur either independently of, or in conjunction with, GATA1. **(F)** Motif enrichment analysis for GATA2-only peaks and peaks bound by both GATA2 and GATA1. GATA2-only peaks are enriched for canonical GATA motifs and RUNX-associated elements, whereas peaks bound by both factors display composite GATA/E-box motifs characteristic of TAL1-centered regulatory assemblies. **(G)** Genomic distribution of GATA2-only peaks versus peaks bound by both GATA2 and GATA1 among Early erythroid–restricted sites. GATA2-only peaks are preferentially promoter-proximal, whereas peaks bound by both factors are enriched at intronic and intergenic regions, supporting distinct promoter- and enhancer-associated regulatory roles during Early erythroid differentiation. Created using *BioRender.com*.

CUT&Tag signal aligned across all Early erythroid–restricted peaks revealed a sharp, centrally enriched GATA2 signal in Early erythroid cells, with minimal signal at the same genomic coordinates in Basal progenitor or Late erythroid populations (Figure 5C). This pattern, **consistent** with the global stage-specific enrichment profiles (Figure Supplement 3), indicates that these sites represent bona fide stage-restricted GATA2 recruitment rather than persistent binding carried across differentiation states. Representative loci illustrate this behavior across distinct genomic contexts, including a promoter-proximal peak near *Nono*, an intronic site within *Nr3c1*, and an intergenic site near *Gata3* (Figure 5D). Across these diverse genomic contexts, spanning promoter-proximal, intronic, and intergenic regions, each locus exhibits a defined GATA2 peak selectively in the Early erythroid state that is lost again in the Late erythroid state.

To determine whether Early erythroid–restricted GATA2 peaks represent a single regulatory category or multiple subclasses, these sites were intersected with GATA1 CUT&Tag data. This analysis resolved two major groups: GATA2-only peaks (~60%, n = 700) and peaks bound by both GATA2 and GATA1 (~40%, n = 467) (Figure 5E). To further characterize these subclasses, we examined their sequence features and genomic annotation. GATA2-only peaks were enriched for canonical GATA motifs and RUNX-associated elements, whereas peaks bound by both GATA2 and GATA1 displayed composite GATA/E-box motifs characteristic of TAL1-centered regulatory assemblies (Figure 5F). Consistent with these motif distinctions, the two subclasses exhibited divergent genomic distributions, with GATA2-only sites showing marked promoter proximity compared to the distal profile of co-bound peaks (Figure 5G).

Together, these analyses indicate that Early erythroid–restricted GATA2 recruitment comprises at least two genomic subclasses defined by transcription factor overlap, motif composition, and genomic annotation. These binding patterns delineate the genomic landscape occupied by GATA2 during Early erythroid differentiation, coinciding with the transitory stage of enhanced chromatin engagement observed by live-cell single-molecule imaging.

Discussion

The findings presented here demonstrate that GATA2 chromatin engagement is dynamically regulated during erythroid differentiation. Rather than decreasing monotonically as GATA1 levels rise, GATA2 engagement exhibits a distinct temporal reorganization, defining an Early erythroid transition state. Across three complementary systems including cell line models as well as primary cells, live-cell single-molecule imaging reveals a transitory strengthening of GATA2 chromatin engagement during erythroid entry. This strengthening is reflected by prolonged apparent residence times in G1E-ER4 cells under matched acquisition conditions and by an expanded long-lived binding population in HPC7 cells and primary bone marrow progenitors. At the late stage of erythroid commitment, GATA2 chromatin engagement declines across all systems. Together, these coordinated kinetic shifts support a model in which transcription factor binding characteristics are dynamic and not unidirectional, following a non-monotonic trajectory that is closely associated with lineage differentiation.

Prior single-molecule studies have established that transcription factors exhibit both short-lived chromatin interactions (<1 s), typically associated with non-specific target search, and longer-lived interactions (multi-second), which correlate with sequence-specific engagement at regulatory elements (Gebhardt et al. 2013; Hansen et al. 2017; Kenworthy et al. 2022). Interpreted within this framework, the expansion of the long-lived GATA2 binding population and prolongation of residence times observed here indicate enhanced specific chromatin engagement during Early erythroid differentiation. Conversely, the predominance of short-lived interactions in progenitor or late stages is consistent with reduced stable regulatory occupancy at lineage-specific elements.

This kinetic perspective adds a further temporal dimension to the classical GATA-switch model, which has been defined primarily by unidirectional changes in expression and genomic occupancy as GATA1 replaces GATA2 (Bresnick et al. 2012; Suzuki et al. 2013). Our single-molecule data identify a discrete phase at the onset of differentiation during which GATA2 chromatin engagement is transiently intensified before displacement. CUT&Tag profiling supports

this framework by identifying regulatory elements occupied by GATA2 only during the Early transition state. These sites segregate into two subclasses: promoter-proximal regions enriched for strong GATA motifs and RUNX1 elements, and distal regions containing composite GATA/E-box motifs characteristic of TAL1-centered enhancer assemblies (May et al. 2013; Tijssen et al. 2011). These subclass-specific features align with known hematopoietic regulatory modules and provide a mechanistic framework for the selective strengthening of GATA2 chromatin engagement at the onset of differentiation.

In this framework, the Early transition state represents a brief phase during which GATA2 increases its engagement with selected regulatory elements before being replaced by GATA1. This model is summarized in Figure 6, which illustrates how GATA2 chromatin engagement is transiently strengthened during early differentiation despite declining protein levels, defining a distinct kinetic phase of the GATA switch. These temporal changes suggest that GATA2 helps establish chromatin configurations that facilitate the subsequent GATA1-driven transcriptional program.

Comparisons across the three experimental systems indicate that the strengthening of GATA2 chromatin engagement during Early erythroid entry is context dependent. G1E-ER4 cells provide a highly synchronized system in which acute GATA1 activation can be precisely controlled. In this setting, Early erythroid entry is associated with prolonged long-lived GATA2 residence times without detectable expansion of the long-lived chromatin-binding population. The absence of a population-level shift may reflect the engineered GATA1-null background and reduced physiological heterogeneity of this system.

In contrast, HPC7 cells and primary erythroid progenitors exhibit distinct kinetic behavior relative to G1E-ER4 cells. These systems comprise heterogeneous progenitor populations in which cytokine signaling and lineage cues regulate endogenous *Gata2* expression. In both contexts, Early erythroid entry was marked by an expansion of the long-lived GATA2 binding population rather than a pronounced change in residence time. This divergence likely reflects differences in chromatin accessibility, cofactor availability, or transcription factor stoichiometry between engineered and native differentiation systems. Despite these quantitative differences, all three systems share a common qualitative pattern: GATA2 chromatin engagement is transiently strengthened during Early erythroid entry and subsequently reduced in the Late stage as differentiation proceeds.

Primary cells displayed features observed in both cell-line models. As in HPC7 cells, primary Early erythroid progenitors exhibited an increased proportion of long-lived chromatin-bound GATA2 molecules. In addition, primary cells showed an Early-stage increase in the residence time of short-lived GATA2 interactions, followed by a reduction at the Late stage, paralleling the residence-time modulation observed in G1E-ER4 cells. Thus, the single-molecule measurements in primary cells capture both an Early expansion of the long-lived binding population and a coordinated modulation of short-lived interaction kinetics.

Because the knock-in allele is subject to endogenous regulatory control, including native promoter usage and physiological protein stoichiometry, these combined effects likely reflect a more complete regulatory landscape than either engineered cell line systems alone. Notwithstanding, a shared kinetic signature emerges across all models: GATA2 chromatin engagement is strengthened during Early erythroid entry and subsequently diminishes as differentiation proceeds. This convergence supports a unified model in which Early erythroid entry is characterized by a previously unappreciated transitory kinetic phase of enhanced GATA2 chromatin interaction.

Of note, single-molecule imaging was essential for resolving the properties of this Early transition state. While prior single-molecule studies examining mRNA indicate that lineage factors are co-expressed and undergo gradual yet reversible quantitative remodeling during hematopoietic priming (Wheat et al., 2020), population-averaged chromatin binding assays cannot determine whether transcription factor–chromatin interactions follow similarly gradual dynamics. Ensemble approaches, including bulk CUT&Tag, measure chromatin occupancy averaged across large cell populations but cannot capture how transcription factor engagement becomes kinetically

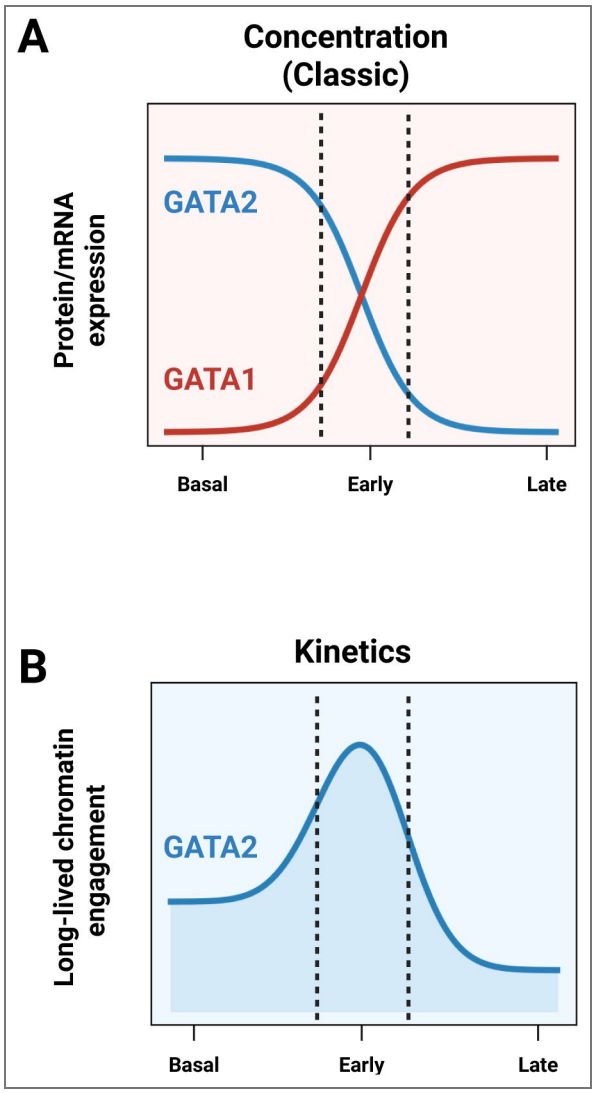

Figure 6. A kinetic transition state uncouples GATA2 chromatin engagement from protein abundance during erythroid differentiation.

(A) Expression Dynamics (Classical View). The canonical model of the GATA switch, where GATA2 protein levels (blue line) decline monotonically as GATA1 levels (red line) rise to drive differentiation. **(B) Chromatin Engagement Dynamics (Kinetic View).** In contrast to expression, single-molecule measurements reveal that GATA2 chromatin engagement (blue line) is transiently strengthened during the Early erythroid transition. This creates a kinetic peak that uncouples binding activity from protein abundance, defining a distinct biophysical phase of lineage commitment. Created using *BioRender.com*.

strengthened or weakened at the single-molecule and single cell levels. By combining live-cell single-molecule tracking with chromatin profiling, our approach revealed regulatory phases that are not readily apparent from population-averaged measurements alone.

Several methodological advances enabled this analysis: (i) CD43-mediated immobilization of non-adherent hematopoietic progenitors, which preserves native nuclear dynamics in suspension cells; (ii) HaloTag and SNAP-tag labeling strategies, which allow detection of low-abundance transcription factors under sparse-labeling conditions; and (iii) live single-cell single molecule tracking, which captures cell-to-cell heterogeneity in chromatin engagement dynamics. Together, these capabilities establish live-cell single-molecule imaging as a powerful framework for dissecting dynamic transcription factor regulation in hematopoietic differentiation.

The CUT&Tag datasets further suggest that early GATA2 binding may have functional consequences for erythroid lineage progression. Promoter-proximal sites uniquely bound by GATA2 may contribute to maintenance of progenitor identity or priming of early erythroid genes, whereas distal elements bound by both GATA2 and GATA1 may reflect regulatory assemblies that facilitate recruitment of TAL1, LMO2, and additional cofactors during commitment. Cooperative interactions among GATA factors, RUNX1, TAL1, and related hematopoietic regulators have been described in multipotent progenitors and early hematopoiesis (Pimanda et al. 2007; Tijssen et al. 2011). In addition, chromatin architectural factors such as the cohesin complex have been implicated in shaping transcription factor occupancy and lineage bias in hematopoietic cells (Tothova et al. 2021; Viny et al. 2019). Together, these observations raise the possibility that the increased GATA2 engagement observed during Early erythroid entry reinforces specific regulatory networks prior to the subsequent dominance of GATA1, providing a plausible mechanistic basis for the transitory kinetic strengthening depicted in our model (Figure 6).

Although the percentage of long-lived GATA2 chromatin engagement falls during commitment, a minority of long-lived interactions persists. These residual events may help sustain enhancer architecture or maintain limited regulatory output, consistent with GATA-factor roles in enhancer assembly and cis-regulatory organization (Bresnick et al. 2012; Oksuz et al. 2023). Determining whether the remaining long-lived interactions in the Late stage erythroid cells help preserve structural features, reinforce silencing, or maintain minimal regulatory functions will be an important direction for future work.

While our study defines a kinetic framework for the GATA switch, several important limitations should be acknowledged. First, GATA2 functions within multi-subunit regulatory complexes, and tracking GATA2 alone may underrepresent the full heterogeneity of chromatin-binding behaviors exhibited by these assemblies. Second, although CUT&Tag profiling identifies stage-specific genomic regions occupied by GATA2, current live-cell single-molecule imaging approaches cannot yet resolve which specific genomic locus corresponds to an individual binding event *in vivo*. This limitation restricts our ability to directly link changes in binding kinetics to specific regulatory elements within single cells during early erythroid differentiation. Third, although we rely on established literature demonstrating declining GATA2 expression during erythroid differentiation, direct quantification of endogenous GATA2 protein abundance in parallel with kinetic measurements will be an important direction for future work. Finally, our interpretation of the relationship between GATA2 and GATA1 relies on population-based staging rather than direct observation of factor exchange at individual chromatin sites. Future studies using simultaneous dual-color single-molecule tracking will be required to visualize the real-time interplay between GATA2 and GATA1 on chromatin and to determine whether GATA1 actively displaces GATA2 or occupies sites only after GATA2 dissociation. Extending these approaches to additional partner factors (e.g., FOG1, TAL1) or targeted perturbation models will be essential for dissecting how specific protein–protein and protein–DNA interactions give rise to the kinetic states described here.

Overall, our findings indicate that transitory non-unidirectional transcription factor kinetics represent an underappreciated dimension of the GATA switch. Similar temporal shifts in chromatin-binding behavior may occur during the initiation and resolution of other lineage

transitions. More broadly, our data demonstrate that single-molecule measurements reveal regulatory phases inaccessible to population-scale methods, establishing transcription factor kinetics as a distinct and critical dimension of lineage differentiation.

Methods

Cell culture and differentiation

G1E-ER4 cells were maintained in Iscove's Modified Dulbecco's Medium (IMDM) supplemented with 15% FBS, 1% penicillin–streptomycin, monothioglycerol (MTG; Sigma), Kit-ligand conditioned medium, and erythropoietin (EPO; PeproTech #554597), following standard protocols (Weiss et al., 1997). EPO was present throughout both maintenance and differentiation. Cells were cultured at 37 °C with 5% CO_2 in suspension and maintained between 1×10^5 and 1×10^6 cells/mL. Erythroid differentiation was initiated with 100 nM 4-hydroxytamoxifen (Sigma #H6278), and cells were collected at Basal (0 h), Early (2 h), and Late (24 h) time points.

HPC7 cells were maintained in IMDM supplemented with 10% FBS, 1% penicillin–streptomycin, 74.8 µM monothioglycerol, and 100 ng/mL stem cell factor (SCF; PeproTech, 300-07). For differentiation, cells were washed and resuspended in medium containing reduced SCF (20 ng/mL) and 4 U/mL EPO according to Sasca et al. (2019). Populations were collected at Basal (0 h, maintenance conditions), Early (2 h post-induction), and Late (24 h post-induction) time points.

Because neither cell line has an established STR reference profile, identity and stability were confirmed by morphology, differentiation behavior, and expression of lineage-appropriate transcription factors. All lines tested negative for mycoplasma (Lonza MycoAlert).

Generation of stable GATA2–HaloTag reporter lines

Stable reporter lines expressing GATA2–HaloTag were generated by lentiviral transduction. The *Gata2*–HaloTag coding sequence was cloned into the pLVX vector upstream of an IRES–ZsGreen reporter and destabilization domain (DD) (Takara #632175). Lentivirus was produced in HEK293T cells by cotransfecting pLVX-GATA2–HaloTag with psPAX2 (Addgene #63586) and pMD2.G (Addgene #12259) using Lipofectamine 2000. Viral supernatants were collected at 48 h. G1E-ER4 and HPC7 cells were transduced on RetroNectin-coated plates (20 µg/mL; Takara #T100A). After 48 h, ZsGreen-positive cells were isolated by FACS and expanded as stable populations. Expression level and nuclear localization of GATA2–HaloTag were validated by live-cell fluorescence microscopy.

Induction of GATA2–HaloTag expression

The DD degron promotes constitutive proteasomal degradation of the fusion protein, necessitating stabilization before imaging. Cells were incubated with 1 µM Shield-1 (Clontech) for 2 h prior to single-molecule acquisition. During the final 20 min of incubation, cells were labeled with 5 nM Janelia Fluor 646 HaloTag Ligand (Promega #GA1120), followed by two washes in warm Leibovitz's L-15 Medium, no phenol red (Gibco #21083027). Shield-1 was used to stabilize the DD-tagged fusion protein prior to imaging and was not applied as an experimental perturbation.

Generation of Gata2–SNAP–STOP–PP7v3 knock-in mouse line

Gata2–SNAP–STOP–PP7v3 knock-in mice were generated using CRISPR/Cas9 genome editing in C57BL/6 zygotes. A donor cassette encoding the SNAP protein, a termination codon, and PP7v3 was inserted immediately downstream of the endogenous *Gata2* coding sequence. Synonymous mutations (P470P, H471H, P472P, S473S) were incorporated into the donor to prevent Cas9 re-cleavage. Founder animals were crossed to wild-type C57BL/6 mice to confirm germline transmission, and heterozygous Gata2–Snap–STOP–PP7v3/+ mice were validated by Sanger sequencing. Animals were subsequently backcrossed to remove potential off-target or random integrations and intercrossed to generate homozygous mice for experimental analysis. All mouse procedures were approved by the Albert Einstein College of Medicine IACUC.

Bone marrow isolation and flow cytometry

Bone marrow was isolated from the femurs and tibias of homozygous GATA2–SNAP mice (n = 2; 12–14 weeks; male and female). Red blood cells were removed using ACK lysis buffer. Cells were stained for CD71 (clone R17217; Thermo Fisher Scientific, #17-0711-82) and Ter119 (clone TER-119; Thermo Fisher Scientific, #48-5921-82) to define erythroid subpopulations: CD71^high^Ter119^low (proerythroblasts), CD71^high^Ter119^intermediate (basophilic erythroblasts), and CD71^low^Ter119^high (committed erythroid cells).

Sorted populations were collected directly into a Ham's F-12–based hematopoietic maintenance medium (Gibco, 11765054) supplemented with 10 mM HEPES, 1× penicillin–streptomycin–glutamine (PSG; Gibco, 10378016), 1× insulin–transferrin–selenium–ethanolamine (ITS-X; Gibco, 51500056), 1 mg/mL polyvinyl alcohol (PVA; Sigma, P8136), 100 ng/mL TPO, and 10 ng/mL SCF, following the short-term HSPC culture conditions described previously (Wilkinson et al. 2020). Cells were incubated overnight in this medium. For single-molecule imaging, cells were labeled with 6 nM SNAP-Cell 647-SiR (NEB #S9102S) for 30 min at 37 °C, followed by two washes in warm L-15 medium. Immediately before live-cell imaging, cells were transferred into L-15 medium supplemented with 100 ng/mL SCF and 10 ng/mL TPO and imaged without further culture.

Microscope acquisition

Immediately prior to imaging, cells were washed in warm L-15 medium and resuspended in L-15 supplemented with 10% FBS and cytokines appropriate for each specific cell state to maintain signaling pathways during acquisition. For G1E-ER4 experiments, imaging medium was supplemented with EPO, with the addition of 100 nM 4-hydroxytamoxifen for Early and Late time points. For HPC7 experiments, imaging medium contained SCF (100 ng/mL for Basal; 20 ng/mL for Early and Late) and 4 U/mL EPO (for Early and Late).

Single-molecule imaging was performed on a Nikon Eclipse Ti microscope equipped with a 150×/1.49 NA oil objective, controlled through VisiView 6.0.0.36 (Visitron Systems). Janelia Fluor® 646 HaloTag® Ligand (Promega #GA1120) or SNAP-Cell® 647-SiR fluorophores were excited using a 639 nm laser, and fluorescence was collected on a Prime 95B sCMOS camera (final pixel size 73 nm). Movies were acquired at 500 ms per frame for >1,000 frames per cell, and a stage-top incubator which maintained samples at 37 °C throughout imaging (Kenworthy et al. 2022).

All movies were acquired under identical illumination power, camera settings, dye concentrations, and preparation conditions across undifferentiated, transitioning, and committed samples, thereby enabling direct comparison of apparent residence time behavior under matched acquisition conditions.

Image preprocessing

Single-molecule TIFF files were organized and pre-processed using custom Python scripts, ImageJ/Fiji macros, and MATLAB code. Raw TIFF stacks were processed to generate photobleaching-control and background-subtracted TIFF files. Background subtraction was performed using a rolling-ball algorithm with a radius of 50 pixels, and output files were saved into standardized condition-specific directories.

Single-particle tracking and analysis

Single-particle tracking was performed using the STRAP (Single-molecule TRacking And Processing) pipeline implemented in MATLAB, as described previously (Haque and Coleman 2025). STRAP incorporates automated implementations of SLIMfast and evalSPT (Sergé et al. 2008; Normanno et al. 2015).

Tracking parameters were matched across all conditions and included a numerical aperture of 1.49, an exposure time of 500 ms, a pixel size of 73 nm, a gap allowance of up to 1.5s, and a maximum diffusion coefficient of 0.05 $\mu m^2/s$. Single-molecule localizations were identified by Gaussian fitting and linked frame-by-frame to generate trajectories.

For each cell, a two-dimensional projection map was generated from the x–y positions of all detected binding events. Nuclear boundaries were defined from this projection, and events occurring outside the nucleus were excluded from downstream analysis. Residence times were extracted for all trajectories and used to classify binding events as transient (<1 s) or stable (>5 s), as described in the main text.

To correct for photobleaching, nuclear fluorescence decay was measured in each cell to determine a per-cell photobleaching lifetime. Apparent residence-time distributions were corrected using a right-censoring model in which the observed off-rate reflects the sum of chromatin dissociation and photobleaching rates. This approach yielded photobleach-adjusted residence-time estimates under constant excitation conditions.

Detailed usage instructions and example workflows for STRAP are provided in the GitHub repository referenced in the Code availability section.

CUT&Tag

CUT&Tag was performed essentially as previously described (Kaya-Okur et al. 2019; Taylor et al. 2024) with minor adaptations for murine progenitors. Approximately 1×10^6 cells were lightly fixed with 2% formaldehyde for 2 min at room temperature, quenched with glycine, and immobilized on ConA magnetic beads activated in 10 mM $CaCl_2$ and 10 mM $MnCl_2$. Samples were incubated overnight at 4 °C with primary antibodies against HaloTag (Promega G9211) or GATA1 (Santa Cruz sc-265) in Dig-Wash (0.01% digitonin), followed by a 1 h room-temperature incubation with secondary antibody. After washing, pA-Tn5 was added for 1 h at room temperature, and tagmentation was initiated by adding 10 mM $MgCl_2$ activation buffer for 60 min at 37 °C. DNA was purified by phenol–chloroform–isoamyl extraction. Indexed libraries were generated with NEBNext HiFi 2× Master Mix and amplified for 13 PCR cycles, followed by 1.2× AMPure cleanup. Libraries were sequenced on an Illumina NextSeq 500 (paired-end, 35 bp). Reads were trimmed and aligned with Bowtie2 using recommended CUT&Tag parameters, and peaks were called with MACS2 ($q < 0.01$, --nomodel --extsize 147). Peak overlaps and stage-restricted sets were computed using bedtools intersect, and heatmaps were generated with deepTools computeMatrix and plotHeatmap. IgG controls were processed in parallel to quantify background and define thresholds during peak calling.

Computational analysis of CUT&Tag peak sets

Aligned BAM files were processed with deepTools (v3.5.1) and bedtools (v2.29.0). MACS2 peak calling used --nomodel --extsize 147 -q 0.01. Transitioning-specific peaks were defined as MACS2 peaks present only in the transitioning state and absent at 0 h and 24 h (bedtools intersect -v).

UpSet-derived regulatory categories

Peak sets from the Basal (0 h), Early (2 h), and Late (24 h) states were compared using bedtools and visualized as an UpSet intersection matrix. Peaks were classified as Basal, Early-only, shared, Early-to-Late, Late-acquired, or monotonic. These categories were used for visualization in Figure 5B.

Signal heatmaps, co-bound classification, and genomic annotation

Signal heatmaps were generated using deepTools computeMatrix (±2 kb around summits) and plotted with plotHeatmap. GATA2-only vs. GATA2+GATA1 bound peaks were determined by intersecting transitioning-specific GATA2 peaks with GATA1 CUT&Tag peaks. Genomic annotations (promoter, intron, exon, intergenic, downstream) were assigned using ChIPseeker.

Motif enrichment analysis

Motif analysis used SeqPos (Cistrome). BED files corresponding to transitioning-only, GATA2-only, GATA2+GATA1 bound, and region-specific subsets were supplied as input. SeqPos identified enriched known and de novo motifs, including high-information GATA sites, RUNX motifs, and

GATA/E-box composite motifs associated with TAL1-dependent enhancers. Genome browser tracks were visualized in IGV 2.16.2.

Western blotting

Cells were lysed in RIPA buffer supplemented with HALT inhibitors (Thermo #78428). Protein concentrations were determined by BCA assay (Pierce #23227). Equal protein amounts were resolved by SDS–PAGE and transferred to PVDF. Membranes were blocked in 5% milk and incubated overnight at 4 °C with primary antibodies against GATA1 (1:1000) and β-actin (1:5000; CST #4967). After secondary incubation with IRDye-conjugated antibodies, blots were imaged on a LI-COR Odyssey CLx and quantified in Image Studio.

Statistical analysis

Single-molecule experiments included at least two biological replicates unless noted. Data are shown as mean ± SEM. Each point represents a single cell. Bars represent mean ± SEM values. Statistical significance was evaluated using the Brown–Forsythe and Welch ANOVA test with Games–Howell post hoc correction. Statistical significance was defined as $P < 0.05$. Significance levels are indicated as follows: *$P < 0.05$; **$P < 0.01$. CUT&Tag analyses were performed in R (v4.3) with Bioconductor tools; peak set comparisons used bedtools.

Figure supplements

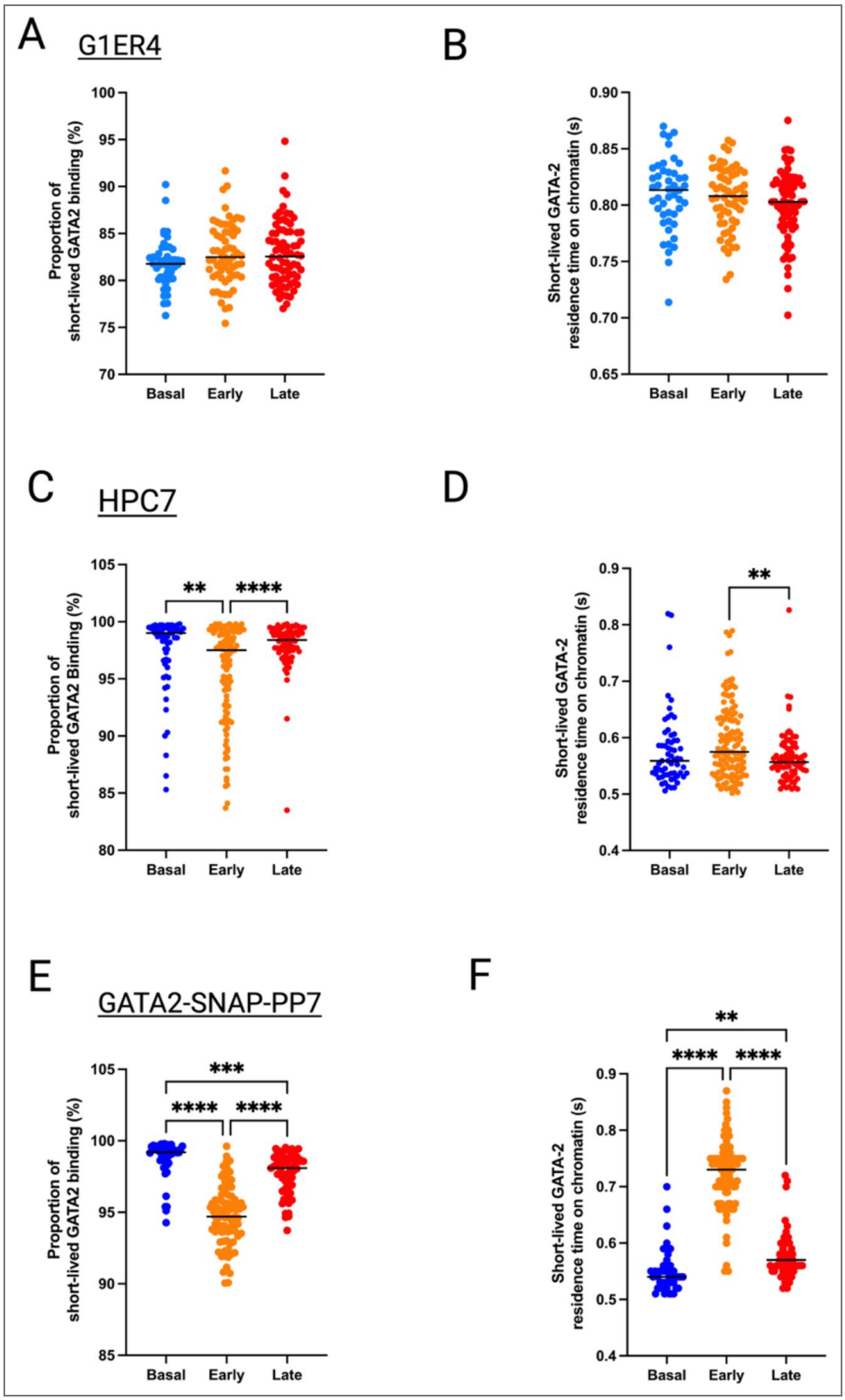

Figure supplement 1. Short-lived GATA2 chromatin binding dynamics across differentiation in G1E-ER4, HPC7, and primary mouse progenitors. (A–B) G1E-ER4 cells. The fraction of short-lived (<1 s) GATA2–Halo interactions and the corresponding short-lived residence times did not differ significantly across the Basal (0 h), Early (2 h), and Late (24 h) stages. **(C–D)** HPC7 progenitors. The short-lived fraction decreased modestly at the

Early (2 h) stage and increased again at the Late (24 h) stage (C). Short-lived residence times declined significantly from the Early to the Late stage (D). **(E–F)** Primary *Gata2*–SNAP bone-marrow progenitors. The short-lived fraction differed across all three stages, with the largest decrease at the Early stage (E). Short-lived residence times increased from Basal to Early cells and decreased again after the Late stage commitment (F). Statistical comparisons used Brown–Forsythe and Welch ANOVA with Games–Howell post-hoc tests. Significance was defined as $P < 0.05$, with significance levels indicated as: * $P < 0.05$; ** $P < 0.01$; *** $P < 0.001$; **** $P < 0.0001$. Created using *BioRender.com*.

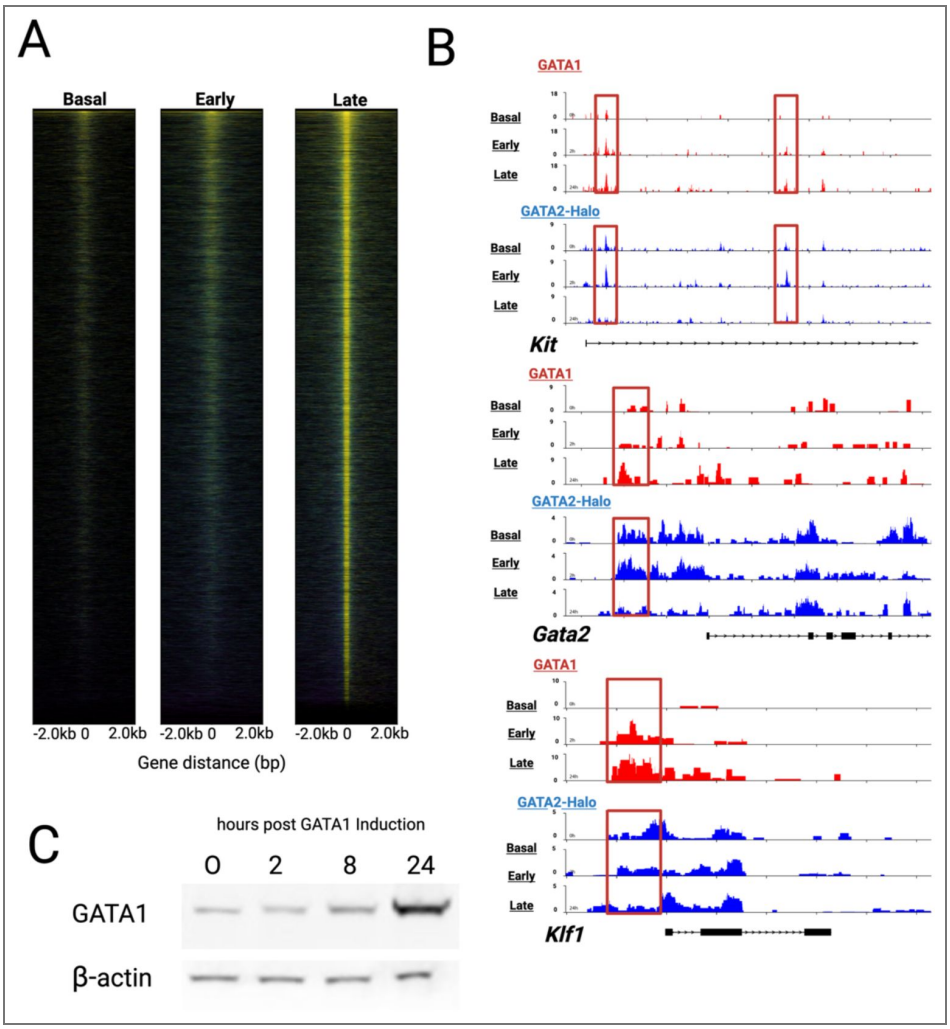

Figure supplement 2. Validation of erythroid induction and GATA factor exchange in the GATA2–Halo reporter line.

These analyses confirm that the GATA2–Halo reporter line undergoes normal erythroid induction and GATA1 activation. **(A)** Heatmap of GATA1 CUT&Tag signal aligned across gene bodies at Basal (0 h), Early (2 h), and Late (24 h) stages following 4-hydroxytamoxifen treatment. Rows are ordered by increasing signal intensity. GATA1 occupancy increases progressively over the time course, with strongest enrichment at 24 h. **(B)** Representative genome-browser views comparing GATA1 (red) and GATA2–Halo (blue) CUT&Tag occupancy at the *Gata2*, *Klf1*, and *Kit* loci. Tracks illustrate progressive gain of GATA1 binding accompanied by a reduction or redistribution of GATA2–Halo occupancy during erythroid progression. Red boxes highlight sites of reciprocal GATA factor exchange ("GATA switch"). Y-axis scales are fixed across time points within each factor to enable direct visual comparison. **(C)** Western blot analysis of GATA1 protein abundance at 0, 2, 8, and 24 h after 4-hydroxytamoxifen treatment. β-actin serves as a loading control. GATA1 protein levels increase over time, with maximal expression at 24 h. Created using *BioRender.com*.

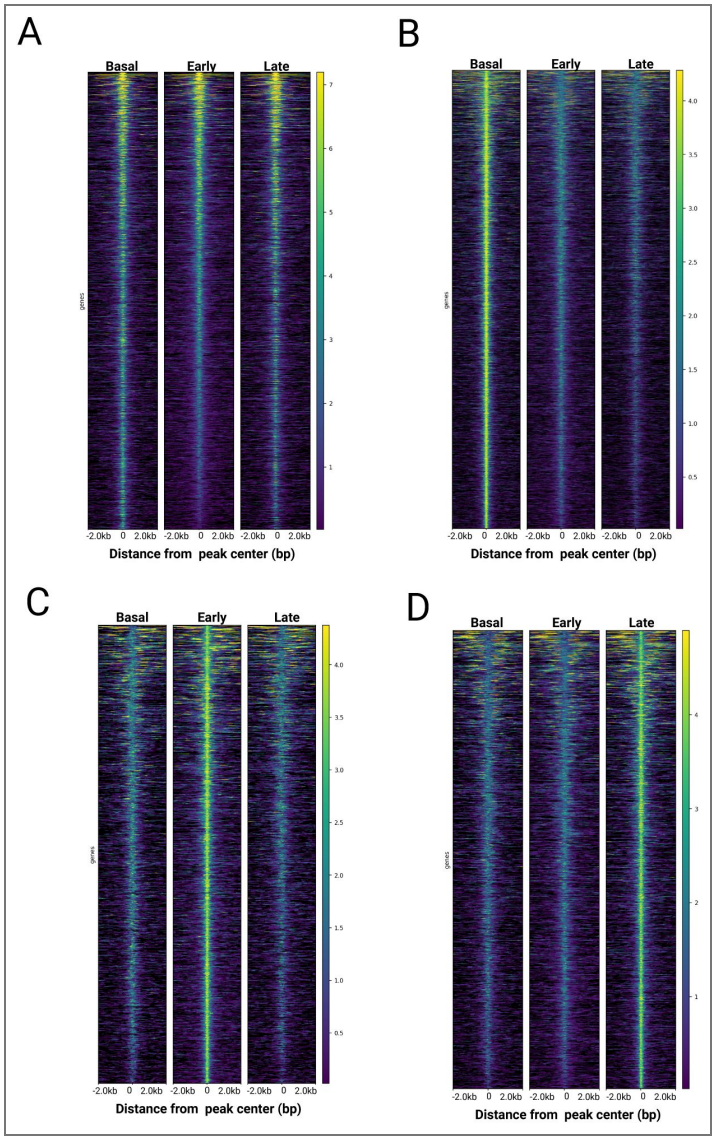

Figure supplement 3. Global CUT&Tag signal patterns across GATA2 peak classes during erythroid differentiation.

CUT&Tag signal heatmaps showing GATA2 occupancy across peak categories defined in Figure 5A, including peaks shared across all stages, Basal progenitor–specific (0 h), Early erythroid–specific (2 h), and Late erythroid–specific (24 h) regions. Heatmaps confirm stage-restricted enrichment and validate the temporal classification of GATA2 binding sites used for downstream analyses. **(A)** All GATA2 peaks. **(B)** Basal progenitor–specific peaks (0 h). **(C)** Early erythroid–specific peaks (2 h). **(D)** Late erythroid–specific peaks (24 h). Created using *BioRender.com*.

Data Availability

The CUT&Tag sequencing data generated in this study have been deposited in the NCBI Gene Expression Omnibus (GEO) and are accessible under accession number GSE318619. Single-molecule tracking datasets and raw movie files are available from the corresponding authors upon reasonable request. Single-molecule imaging data were processed using the STRAP (Single-molecule TRacking And Processing) pipeline (Haque and Coleman 2025). STRAP was used for image preprocessing, single-particle tracking, and downstream trajectory analysis. The STRAP scripts are publicly available under the GNU General Public License v3.0 at *https://github.com/codedbynayem*. Detailed usage instructions are provided in the repository.

Acknowledgements

We thank Daqian Sun and Jaime Clark from the Flow Cytometry Core at the Ruth L. and David S. Gottesman Institute for Stem Cell Biology and Regenerative Medicine at Albert Einstein College of Medicine for assistance with cell sorting. We also thank Yongwei Zhang of the Gene Targeting and Transgenic Facility for generating the mouse lines used in this study. The authors would like to acknowledge the input and support of all members of the Steidl and Coleman laboratories. This work was supported by a grant from the National Institutes of Health (NIH), including NIGMS R01GM126045 awarded to R.A.C., and NCI R35CA253127 awarded to U.S., as well as V Foundation grant AST2025-007 (awarded to U.S.). R.K. was supported by a Career Development Fellowship from Blood Cancer United. S.J.T. was supported by a Young Investigator award from the Edward P. Evans Foundation. U.S. holds the Edward P. Evans Endowed Professorship in Myelodysplastic Syndromes at Albert Einstein College of Medicine. The Endowed Professorship was supported by a grant from the Edward P. Evans Foundation. Also, this work was supported by Jane A. and Myles P. Dempsey. This work was also supported by NIH NIGMS training grant T32GM007491 and the New York Consortium for Interdisciplinary Training in Kidney, Urological and Hematological Research (NYC Train KUHR) award TL1DK136048 to J.W.H. Schematic diagrams were created with BioRender.com. Grammarly was used for language editing and proofreading during the preparation of this manuscript.

Additional information

Author contributions

John W Hobbs: Conceptualization, Methodology, Resources, Investigation, Validation, Data curation, Formal analysis, Visualization, Funding acquisition, Writing- Original Draft, Writing- Review and Editing

Samuel J Taylor: Conceptualization, Investigation, Data curation, Formal analysis, Visualization, Writing- Review and Editing

Rajni Kumari: Conceptualization, Resources, Investigation, Formal analysis, Visualization, Writing- Review and Editing

Nayem Haque: Methodology, Software, Writing- Review and Editing

Lou Lou Victor Jagaraja: Resources, Investigation

Ulrich Steidl: Conceptualization, Resources, Validation, Formal analysis, Visualization, Funding acquisition, Supervision, Writing- Original Draft, Writing- Review and Editing, Project administration

Robert A. Coleman: Conceptualization, Resources, Validation, Formal analysis, Visualization, Funding acquisition, Supervision, Writing- Original Draft, Writing- Review and Editing, Project administration

Funding

Funder	Grant reference number	Author
National Institute of General Medical Sciences	R01GM126045	Robert A Coleman
National Cancer Institute	R35CA253127	Ulrich Steidl
National Cancer Institute	P30CA013330	Ulrich Steidl
V Foundation for Cancer Research (VFCR)	AST2025-007	Ulrich Steidl
National Science Foundation	GRFP FAIN-2437848	Nayem Haque
National Institute of General Medical Sciences	T32GM007491	John W Hobbs
National Institute of Diabetes and Digestive and Kidney Diseases	TL1DK136048	John W Hobbs

Author ORCID iDs

John W Hobbs: https://orcid.org/0000-0003-1870-5861
Nayem Haque: https://orcid.org/0000-0003-1912-4401
Robert A Coleman: https://orcid.org/0000-0002-7367-9603

Additional files

Supplemental Video 1. Shield-1–dependent accumulation of GATA2–Halo in live HPC7 cells. Live-cell fluorescence imaging of HPC7 cells expressing GATA2–Halo–DD labeled with Janelia Fluor® 646 HaloTag® Ligand (green) and counterstained with SPY555-DNA (blue). The split-screen movie compares cells treated with vehicle control (*Left*) versus 1 μM Shield-1 for 2 hours (*Right*). In the vehicle-treated condition (left), little to no GATA2–Halo fluorescence is detected, consistent with proteasomal degradation of the fusion protein. In contrast, Shield-1 treatment (*Right*) restores robust nuclear accumulation of GATA2–Halo without altering nuclear morphology. Movies represent single optical sections acquired under identical illumination and display settings.

Supplementary Video 2. Representative single-molecule tracking of GATA2-Halo in G1E-ER4 cells. Example single-molecule tracking movie illustrating GATA2 chromatin interactions in G1E-ER4 erythroid progenitor cells. Movie shown at 15 fps.

Supplementary Video 3. Representative single-molecule tracking of GATA2-Halo in HPC7 cells. Example single-molecule tracking movie illustrating GATA2-Halo chromatin interactions in HPC7 cells. Movie shown at 15 fps.

Supplementary Video 4. Representative single-molecule tracking of GATA2-SNAP in primary mouse bone marrow cells. Example single-molecule tracking of GATA2 in primary erythroid progenitors isolated from mouse bone marrow. Movie shown at 15 fps.

References

1. **Ahmed N.**, Kunz L., Hoppe P.S., Loeffler D., Etzrodt M., Ortega G.C., Hilsenbeck O., Anastassiadis K., Schroeder T (2020) A novel GATA2 protein reporter mouse reveals hematopoietic progenitor cell types. *Stem Cell Reports* **15**:326-339 https://doi.org/10.1016/j.stemcr.2020.06.008 | PubMed
2. **Bresnick E.H.**, Katsumura K.R., Lee H.Y., Johnson K.D., Perkins A.S (2012) Master regulatory GATA transcription factors: mechanistic principles and emerging links to hematologic malignancies. *Nucleic Acids Research* **40**:5819-5831 https://doi.org/10.1093/nar/gks281 | PubMed
3. **Fujiwara T.**, O'Geen H., Keles S., Blahnik K., Linnemann A.K., Kang Y.A., Choi K., Farnham P.J., Bresnick E.H (2009) Discovering hematopoietic mechanisms through genome-wide analysis of GATA factor chromatin occupancy. *Molecular Cell* **36**:667-681 https://doi.org/10.1016/j.molcel.2009.11.001 | PubMed

4. **Gebhardt J.C.,** Suter D.M., Roy R., Zhao Z.W., Chapman A.R., Basu S., Maniatis T., Xie X.S (2013) Single-molecule imaging of transcription factor binding to DNA in live mammalian cells. *Nature Methods* **10**:421-426 https://doi.org/10.1038/nmeth.2411 | PubMed

5. **Hansen A.S.,** Pustova I., Cattoglio C., Tjian R., Darzacq X (2017) CTCF and cohesin regulate chromatin loop stability with distinct dynamics. *eLife* **6**:e25776 https://doi.org/10.7554/eLife.25776 | PubMed

6. **Haque N.,** Coleman R.A (2025) Dynamic transcription pre-initiation complex assembly governs initiation efficiency. *bioRxiv* https://doi.org/10.1101/2025.05.07.652662 | PubMed

7. **Heinz S.,** Romanoski C.E., Benner C., Glass C.K (2015) The selection and function of cell type-specific enhancers. *Nature Reviews Molecular Cell Biology* **16**:144-154 https://doi.org/10.1038/nrm3949 | PubMed

8. **Homan C.C.,** Venugopal P., Arts P., Shahrin N.H., Feurstein S., Rawlings L., Lawrence D.M., Andrews J., King-Smith S.L., Harvey N.L., *et al.* (2021) GATA2 deficiency syndrome: A decade of discovery. *Human Mutation* **42**:1399-1421 https://doi.org/10.1002/humu.24271 | PubMed

9. **Johnson K.D.,** Conn D.J., Shishkova E., Katsumura K.R., Liu P., Shen S., Ranheim E.A., Kraus S.G., Wang W., Calvo K.R., *et al.* (2020) Constructing and deconstructing GATA2-regulated cell fate programs to establish developmental trajectories. *Journal of Experimental Medicine* **217** https://doi.org/10.1084/jem.20191526 | PubMed

10. **Katsumura K.R.,** Bresnick E.H., GATA Factor Mechanisms Group (2017) The GATA factor revolution in hematology. *Blood* **129**:2092-2102 https://doi.org/10.1182/blood-2016-09-687871 | PubMed

11. **Kaya-Okur H.S.,** Wu S.J., Codomo C.A., Pledger E.S., Bryson T.D., Henikoff J.G., Ahmad K., Henikoff S (2019) CUT&Tag for efficient epigenomic profiling of small samples and single cells. *Nature Communications* **10**:1930 https://doi.org/10.1038/s41467-019-09982-5 | PubMed

12. **Kenworthy C.A.,** Haque N., Liou S.H., Chandris P., Wong V., Dziuba P., Lavis L.D., Liu W.L., Singer R.H., Coleman R.A (2022) Bromodomains regulate dynamic targeting of the PBAF chromatin-remodeling complex to chromatin hubs. *Biophysical Journal* **121**:1738-1752 https://doi.org/10.1016/j.bpj.2022.03.027 | PubMed

13. **Lambert S.A.,** Jolma A., Campitelli L.F., Das P.K., Yin Y., Albu M., Chen X., Taipale J., Hughes T.R., Weirauch M.T (2018) The human transcription factors. *Cell* **172**:650-665 https://doi.org/10.1016/j.cell.2018.01.029 | PubMed

14. **Laurenti E.,** Göttgens B (2018) From haematopoietic stem cells to complex differentiation landscapes. *Nature* **553**:418-426 https://doi.org/10.1038/nature25022 | PubMed

15. **Levine M.,** Cattoglio C., Tjian R (2014) Looping back to leap forward: transcription enters a new era. *Cell* **157**:13-25 https://doi.org/10.1016/j.cell.2014.02.009 | PubMed

16. **Liu Z.,** Legant W.R., Chen B.C., Li L., Grimm J.B., Lavis L.D., Betzig E., Tjian R (2014) 3D imaging of Sox2 enhancer clusters in embryonic stem cells. *eLife* **3**:e04236 https://doi.org/10.7554/eLife.04236 | PubMed

17. **Loeffler D.,** Wang W., Hopf A., Hilsenbeck O., Bourgine P.E., Rudolf F., Martin I., Schroeder T (2018) Mouse and human HSPC immobilization in liquid culture by CD43-or CD44-antibody coating. *Blood* **131**:1425-1429 https://doi.org/10.1182/blood-2017-07-794131 | PubMed

18. **Los G.V.,** Encell L.P., McDougall M.G., Hartzell D.D., Karassina N., Zimprich C., Wood M.G., Learish R., Ohana R.F., Urh M., *et al.* (2008) HaloTag: a novel protein labeling technology for cell imaging and protein analysis. *ACS Chemical Biology* **3**:373-382 https://doi.org/10.1021/cb800025k | PubMed

19. **May G.,** Soneji S., Tipping A.J., Teles J., McGowan S.J., Wu M., Guo Y., Fugazza C., Brown J., Karlsson G., *et al.* (2013) Dynamic analysis of gene expression and genome-wide transcription factor binding during lineage specification of multipotent progenitors. *Cell Stem Cell* **13**:754-768 https://doi.org/10.1016/j.stem.2013.09.003 | PubMed

20. **Morisaki T.,** Lyon K., DeLuca K.F., DeLuca J.G., English B.P., Zhang Z., Lavis L.D., Grimm J.B., Viswanathan S., Looger L.L., *et al.* (2016) Real-time quantification of single RNA translation dynamics in living cells. *Science* **352**:1425-1429 https://doi.org/10.1126/science.aaf0899 | PubMed

21. **Normanno D.,** Boudarène L., Dugast-Darzacq C., Chen J., Richter C., Proux F., Bénichou O., Voituriez R., Darzacq X., Dahan M (2015) Probing the target search of DNA-binding proteins in mammalian cells using TetR as model searcher. *Nature Communications* **6**:7357 https://doi.org/10.1038/ncomms8357 | PubMed

22. **Oksuz O.,** Henninger J.E., Warneford-Thomson R., Zheng M.M., Erb H., Vancura A., Overholt K.J., Hawken S.W., Banani S.F., Lauman R., *et al.* (2023) Transcription factors interact with RNA to regulate genes. *Molecular Cell* **83**:2449-2463 https://doi.org/10.1016/j.molcel.2023.06.012 | PubMed

23. **Orkin S.H.,** Zon L.I (2008) Hematopoiesis: an evolving paradigm for stem cell biology. *Cell* **132**:631-644 https://doi.org/10.1016/j.cell.2008.01.025 | PubMed

24. **Palii C.G.,** Cheng Q., Gillespie M.A., Shannon P., Mazurczyk M., Napolitani G., Price N.D., Ranish J.A., Morrissey E., Higgs D.R., *et al.* (2019) Single-cell proteomics reveal that quantitative changes in co-expressed lineage-specific transcription factors determine cell fate. *Cell Stem Cell* **24**:812-825 https://doi.org/10.1016/j.stem.2019.02.006 | PubMed

25. **de Pater E.,** Kaimakis P., Vink C.S., Yokomizo T., Yamada-Inagawa T., van der Linden R., Kartalaei P.S., Camper S.A., Speck N., Dzierzak E. (2013) Gata2 is required for HSC generation and survival. *Journal of Experimental Medicine* **210**:2843-2850 https://doi.org/10.1084/jem.20130751

26. **Pimanda J.E.,** Ottersbach K., Knezevic K., Kinston S., Chan W.Y., Wilson N.K., Landry J.R., Wood A.D., Kolb-Kokocinski A., Green A.R., *et al.* (2007) Gata2, Fli1, and Scl form a recursively wired gene-regulatory circuit during early hematopoietic development. *Proceedings of the National Academy of Sciences* **104**:17692-17697 https://doi.org/10.1073/pnas.0707045104 | PubMed

27. **Ross J.,** Mavoungou L., Bresnick E.H., Milot E (2012) GATA-1 utilizes Ikaros and polycomb repressive complex 2 to suppress Hes1 and to promote erythropoiesis. *Molecular and Cellular Biology* **32**:3624-3638 https://doi.org/10.1128/mcb.00163-12 | PubMed

28. **Sasca D.,** Yun H., Giotopoulos G., Szybinski J., Evan T., Wilson N.K., Gerstung M., Gallipoli P., Green A.R., Hills R., *et al.* (2019) Cohesin-dependent regulation of gene expression during differentiation is lost in cohesin-mutated myeloid malignancies. *Blood* **134**:2195-2208 https://doi.org/10.1182/blood.2019001553 | PubMed

29. **Sergé A.,** Bertaux N., Rigneault H., Marguet D (2008) Dynamic multiple-target tracing to probe spatiotemporal cartography of cell membranes. *Nature Methods* **5**:687-694 https://doi.org/10.1038/nmeth.1233 | PubMed

30. **Spinner M.A.,** Sanchez L.A., Hsu A.P., Shaw P.A., Zerbe C.S., Calvo K.R., Arthur D.C., Gu W., Gould C.M., Brewer C.C., *et al.* (2014) GATA2 deficiency: a protean disorder of hematopoiesis, lymphatics, and immunity. *Blood* **123**:809-821 https://doi.org/10.1182/blood-2013-07-515528 | PubMed

31. **Suzuki M.,** Kobayashi-Osaki M., Tsutsumi S., Pan X., Ohmori S., Takai J., Moriguchi T., Ohneda O., Ohneda K., Shimizu R., *et al.* (2013) GATA factor switching from GATA2 to GATA1 contributes to erythroid differentiation. *Genes to Cells* **18**:921-933 https://doi.org/10.1111/gtc.12086 | PubMed

32. **Taylor S.J.,** Stauber J., Bohorquez O., Tatsumi G., Kumari R., Chakraborty J., Bartholdy B.A., Schwenger E., Sundaravel S., Farahat A.A., *et al.* (2024) Pharmacological restriction of genomic binding sites redirects PU.1 pioneer transcription factor activity. *Nature Genetics* **56**:2213-2227 https://doi.org/10.1038/s41588-024-01911-7 | PubMed

33. **Tijssen M.R.,** Cvejic A., Joshi A., Hannah R.L., Ferreira R., Forrai A., Bellissimo D.C., Oram S.H., Smethurst P.A., Wilson N.K., *et al.* (2011) Genome-wide analysis of simultaneous GATA1/2, RUNX1, FLI1, and SCL binding in megakaryocytes identifies hematopoietic regulators. *Developmental Cell* **20**:597-609 https://doi.org/10.1016/j.devcel.2011.04.008 | PubMed

34. **Tothova Z.,** Valton A.L., Gorelov R.A., Vallurupalli M., Krill-Burger J.M., Holmes A., Landers C.C., Haydu J.E., Malolepsza E., Hartigan C., *et al.* (2021) Cohesin mutations alter DNA damage repair and chromatin structure and create therapeutic vulnerabilities in MDS/AML. *JCI insight* **6**:e142149 https://doi.org/10.1172/jci.insight.142149 | PubMed

35. **Tsai F.Y.,** Orkin S.H (1997) Transcription factor GATA-2 is required for proliferation/survival of early hematopoietic cells and mast cell formation, but not for erythroid and myeloid terminal differentiation. *Blood* **89**:3636-3643 https://doi.org/10.1182/blood.v89.10.3636.3636_3636_3643 | PubMed

36. **Tsai F.Y.,** Keller G., Kuo F.C., Weiss M., Chen J., Rosenblatt M., Alt F.W., Orkin S.H (1994) An early haematopoietic defect in mice lacking the transcription factor GATA-2. *Nature* **371**:221-226 https://doi.org/10.1038/371221a0 | PubMed

37. **Viny A.D.,** Bowman R.L., Liu Y., Lavallée V.P., Eisman S.E., Xiao W., Durham B.H., Navitski A., Park J., Braunstein S., *et al.* (2019) Cohesin Members Stag1 and Stag2 Display Distinct Roles in Chromatin Accessibility and Topological Control of HSC Self-Renewal and Differentiation. *Cell Stem Cell* **25**:682-696 https://doi.org/10.1016/j.stem.2019.08.003 | PubMed

38. **Weiss M.J.,** Yu C., Orkin S.H (1997) Erythroid-cell-specific properties of transcription factor GATA-1 revealed by phenotypic rescue of a gene-targeted cell line. *Molecular and Cellular Biology* **17**:1642-1651 https://doi.org/10.1128/mcb.17.3.1642 | PubMed

39. **Wheat J.C.,** Sella Y., Willcockson M., Skoultchi A.I., Bergman A., Singer R.H., Steidl U (2020) Single-molecule imaging of transcription dynamics in somatic stem cells. *Nature* **583**:431-436 https://doi.org/10.1038/s41586-020-2432-4 | PubMed

40. **Wilkinson A.C.,** Ishida R., Nakauchi H., Yamazaki S (2020) Long-term ex vivo expansion of mouse hematopoietic stem cells. *Nature Protocols* **15**:628-648 https://doi.org/10.1038/s41596-019-0263-2 | PubMed

41. **Wlodarski M.W.,** Collin M., Horwitz M.S (2017) GATA2 deficiency and related myeloid neoplasms. *Seminars in Hematology* **54**:81-86 https://doi.org/10.1053/j.seminhematol.2017.05.002 | PubMed

42. **Yamamoto M.,** Ko L.J., Leonard M.W., Beug H., Orkin S.H., Engel J.D (1990) Activity and tissue-specific expression of the transcription factor NF-E1 multigene family. *Genes and Development* **4**:1650-62 https://doi.org/10.1101/gad.4.10.1650 | PubMed

Peer reviews

Reviewer #1 (Public review):

Summary:

During erythroid differentiation, hematopoietic progenitors relinquish multipotency and activate lineage programs. The switch from GATA2 to GATA1 is particularly important in this process, yet GATA2 chromatin-binding kinetics remain undefined. The authors investigated GATA2-chromatin interaction dynamics during erythroid differentiation in three different cell systems using single-molecule live-cell imaging, and they also used CUT&Tag to profile GATA2 chromatin occupancy.

By single-molecule imaging, the authors report two interaction modes for GATA2: short-lived (<1 s) and long-lived (>5 s) binding. The proportion of long-lived molecules, the number of binding events, and the duration of long-lived binding change (or are maintained) during differentiation. Notably, long-lived chromatin engagement by GATA2 increases during early erythroid differentiation and decreases at the late stage. CUT&Tag identifies regulatory elements selectively occupied by GATA2 during the early transition stage. Together, these results support a model in which transcription factor kinetics form a dynamic chromatin-engagement profile that characterizes the GATA2-to-GATA1 transition.

Strengths:

(1) Characterizing transcription-factor binding kinetics during the GATA2->GATA1 transition addresses a fundamental mechanism in erythroid differentiation.

(2) Combining single-molecule live imaging with CUT&Tag provides both dynamic and locus-specific perspectives.

(3) Single-molecule analysis across three different cell systems strengthens the potential generalizability of the findings and highlights biological variability.

Weaknesses:

I agree that single-molecule imaging is a powerful approach for investigating GATA2 kinetics, but the single-molecule data are the most important part of the paper and need improvement. The analyses focus on three measures: (i) duration of long binding, (ii) proportion of short- and long-binding molecules, and (iii) total binding events. However, several methodological and control issues limit confidence in the kinetic interpretations. The authors should address the following major concerns.

(1) Two binding states: justification and controls

The authors propose two states of GATA2 binding. Are there only two states? Studies that separate short- and long-lived binding (e.g., Chen et al., 2014, PMID: 25342811) address two states of transcriptional factors very carefully. Some long-binding duration distributions here are very long-tailed (e.g., Figure 2D middle), suggesting a possible third state. The authors must explain how they determined that two states provide the "best fit" to the data and how they classified "short" versus "long" binding.

Controls should be included for long-lived and short-lived binding (e.g., histone proteins, HaloTag-NLS, or a binding-deficient GATA2 mutant) as in other studies. These controls are essential to exclude alternative explanations (see points below).

(2) Exclude photophysical and focal-plane artifacts

The authors should exclude contributions from (i) photobleaching, (ii) blinking, and (iii) Z-axis motion (disappearance from the focal plane). Although photobleaching correction is mentioned in the Methods, no details are provided. Describe and quantify the photobleaching correction and demonstrate that it was applied across all cell types and conditions.

Some spots in the supplementary movies appear to blink or to move substantially between frames. Provide analyses or controls that distinguish true dissociation events from photophysical blinking/bleaching or axial motion.

(3) HILO illumination and nuclear region sampled

HILO is powerful but sensitive to illumination angle: slight changes sample different nuclear regions (e.g., nuclear interior versus periphery). The nuclear periphery is enriched in heterochromatin and may bias binding statistics. Explain how the authors controlled the HILO angle and confirmed that comparable nuclear regions were imaged across cells and conditions.

(4) Quantification of event counts and long-binding durations

The number of binding events and measured long-binding durations are strongly affected by imaging conditions (labeling/staining, bleaching, nucleus size, cell cycle state, focal plane, spot detectability, etc.). Imaging clarity appears to differ among cells/conditions in the supplementary movie. Provide more careful analysis describing how these variables were controlled or corrected for, and assess the sensitivity of results to choices in detection and tracking parameters.

(5) Evidence that spots are single molecules

The authors state that spots represent single molecules but do not provide supporting evidence. Spot brightness varies considerably in the movies. Brightness differences may reflect axial position. Provide evidence supporting single-molecule assignment (e.g., single-step photobleaching traces, brightness distributions compared to a known single-molecule control, or photon count analysis).

(6) Description of spot-analysis pipeline

The manuscript lacks a sufficient description of the spot-analysis method. I reviewed the STRAP pipeline paper cited (Haque and Coleman 2025 bioRxiv) and the GitHub code, but the Methods in the current manuscript should include a detailed STRAP pipeline. This would enable readers to evaluate and reproduce the analyses.

(7) Differences among cell systems

The three cell systems yield notably different results (e.g., Figure 2C vs 4C and Figure 2D/3D vs 4D). Provide a more detailed explanation for these differences and discuss how biological variability, technical differences, or imaging biases might account for the discrepancies.

https://doi.org/10.7554/eLife.111233.1.sa3

Reviewer #2 (Public review):

In this study, the authors address the molecular mechanism underlying the transcriptional changes during erythroid differentiation from hematopoietic progenitor cells. The authors combine single-molecule live cell imaging and CUT&RUN to analyze the chromatin binding properties of the GATA2 transcription factor prior to and after initiation of differentiation into the erythroid cell lineage. Using three distinct cellular systems, the authors demonstrate that the chromatin binding of GATA2 is transiently increased early in the differentiation process, as evidenced by increased chromatin binding residence time and the emergence of new genomic binding sites identified by CUT&RUN. The strength of the study lies in the combination of single-molecule imaging, which reports on binding dynamics but is agnostic of the binding site, with CUT&RUN, which reports on the binding sites but does not provide dynamic information. The authors clearly demonstrate that chromatin binding of GATA2 is altered early in the differentiation process and is later displaced as cells switch to expression of GATA1, which has been previously observed. The use of three distinct cell lines, in particular the GATA2-SNAP mouse model, is a strength in principle; however, the results are not fully consistent between the different cell systems. A key difference is that the G1E-ER4 and HPC7 cell line models express HaloTagged GATA2 in addition to the endogenous GATA2 protein. The authors go through great lengths to control GATA2-HaloTag expression levels, but they use polyclonal cell lines and do not analyze expression levels of the GATA2-HaloTag transgene, which is a key variable in interpreting their experimental results. Finally, a key variable determined in their single-molecule analysis is the number of binding events observed during the distinct differentiation changes. The number of binding events observed is influenced by the expression level of the tagged protein, which in turn is controlled by the Shield-1 ligand, and the fraction of molecules labeled with the HaloTag ligand. Since transgene protein levels and the labeling efficiency were not determined, it is hard to assess how reliable the measurements of the number of binding events are across all cell lines.

To address the weaknesses summarized above the authors could take the following steps:

(1) Determine the expression levels of the GATA2-HaloTag transgene over the course of differentiation under the conditions used for single-molecule imaging. This will not only allow them to determine the expression of the transgene but also the endogenous untagged protein with which the GATA2-HaloTag fusion proteins compete for binding sites.

(2) To determine the fraction of molecules labeled during imaging, the authors could carry out a titration of the HaloTag ligand and compare the amount of labeled protein under single-molecule imaging conditions to that of saturating labeling of the HaloTag. This approach will ensure that the number of labeled molecules per cell is comparable across experimental conditions and allow the authors to draw more solid conclusions regarding the number of binding events.

(3) The analysis of residence times using single-molecule imaging requires robust single-particle tracking without gaps or interruptions of trajectories. The authors should show images of their particle trajectories to demonstrate that their tracking is robust. Or even better, movies superimposing the trajectories onto the imaging data.

https://doi.org/10.7554/eLife.111233.1.sa2

Reviewer #3 (Public review):

Hobbs et al. use live-cell single-molecule tracking (SMT) of HaloTag- and SNAP-tagged GATA2 combined with CUT&Tag chromatin profiling to examine how GATA2 chromatin engagement evolves during erythroid differentiation. Across three complementary systems, G1E-ER4 cells, HPC7 cells, and primary bone marrow progenitors from a new Gata2-SNAP knock-in mouse, they report a transient strengthening of long-lived GATA2 chromatin binding at the "Early" (2 h) erythroid stage, manifested either as increased residence time (G1E-ER4) or expansion of the long-lived bound fraction (HPC7, primary cells). CUT&Tag identifies 1,167 Early-restricted GATA2 peaks partitioning into GATA2-only (promoter-proximal, GATA/RUNX motifs) and GATA2+GATA1 co-bound (distal, GATA/E-box motifs) subclasses. The authors propose that this kinetic phase represents a previously unappreciated dimension of the GATA switch.

This is a strong study with a genuinely novel finding-the non-monotonic kinetic behavior of GATA2 during erythroid priming, supported by complementary measurements in three biological systems. The issues below are largely clarifications, additional analyses of existing data, and modest refinements to the discussion. With these addressed, the manuscript will make a valuable contribution. I recommend a minor revision.

Specific points:

(1) Clarify the photobleaching correction and report per-cell bleach lifetimes.

The long-lived residence time claim in G1E-ER4 cells depends on careful accounting for photobleaching, which the Methods indicate was done via a right-censoring model. For reviewer and reader confidence, the authors should report the per-stage (or per-cell distribution of) photobleaching lifetimes and the photobleach-corrected residence time values alongside the apparent values in Figure 2D. If feasible, including a brief supplementary analysis with an H2B-Halo or similar long-lived control under matched conditions would further solidify the quantitative claims. This is an analysis of existing data and should not require new imaging.

(2) Unify or explicitly discuss the mechanistic differences across systems.

The three systems show qualitatively different signatures: residence time change in G1E-ER4, bound fraction expansion in HPC7, and primary cells. The authors currently group these under "enhanced engagement," but these signatures imply different underlying mechanisms (koff decrease vs. increased kon or increased specific-binding-competent pool). The Discussion partially addresses this by noting engineered vs. native differences, but a more explicit framing in both Results and Discussion would help readers. Specifically, reporting an on-rate proxy (for example, binding events per unit time normalized to detectable molecule

number) alongside koff would let readers see how the mechanistic pieces fit together. I do not think this changes the central message; it sharpens it.

(3) Per-cell GATA2 concentration would strengthen the "uncoupling" claim.

A central claim of the Figure 6 model is that chromatin engagement is uncoupled from protein abundance. The ectopic Shield-1 stabilization system is a reasonable design choice, but quantifying total nuclear GATA2-Halo signal (for example, from the pre-bleach frame or a brief high-power acquisition) on a per-cell basis across stages would directly support the interpretation. For the primary cells, where the biological claim is strongest, a western blot or quantitative immunofluorescence on the flow-sorted populations would make the uncoupling argument much more defensible. I recognize this may be one additional experiment, but it is a high-value one.

(4) Additional single-cell distribution analysis.

Figure 1E and Figures 2 to 4 show substantial cell-to-cell heterogeneity, and the Early populations in particular look potentially bimodal. Given that the authors cite Wheat et al. and Palii et al. on probabilistic hematopoietic transitions, a brief supplementary analysis using distribution-based statistics (K-S test, or mixture model) rather than, or alongside, mean-based ANOVA would align the analysis with this conceptual framing and may reveal whether the Early state represents a subpopulation transition rather than a uniform shift. This is purely an analysis of existing data.

(5) Quantitative integration of CUT&Tag with SMT.

The manuscript presents SMT and CUT&Tag as complementary but does not attempt to quantitatively connect them. A back-of-the-envelope calculation of whether a 21% increase in residence time (G1E-ER4), or the fraction expansion in other systems, is consistent with the acquisition of the 1,167 Early-restricted sites, given plausible site affinities, would substantially strengthen integration. Even if the calculation is approximate, framing it explicitly would help readers appreciate that the two datasets reinforce each other.

(6) Short-lived kinetic interpretation and tracking parameters.

The 1.5 s gap allowance in tracking is long relative to the 0.55 to 0.73 s short-lived residence times reported in primary cells (Figure Supplement 1F), which could affect the interpretation of the "slowing of target search" claim. A brief sensitivity analysis with tighter gap parameters in the supplement would reassure readers that this effect is robust. Additionally, please clarify how the inferred slowing of search, which should reduce kon, is reconciled with the increased number of binding events per cell at the Early stage.

(7) CUT&Tag peak definition.

The Early-restricted peak set is defined by presence and absence at q less than 0.01, which can be sensitive to near-threshold peaks. Please report either (a) the CUT&Tag signal intensity distribution at the 1,167 sites across all three stages as a quantitative scatter or density plot, beyond the heatmap in Figure 5C, or (b) the result of a differential binding analysis (for example, DESeq2 on read counts in a union peak set) as a supplementary confirmation. Please also state the number of CUT&Tag replicates per stage and the overlap of Early-restricted sets across replicates.

(8) Knock-in mouse validation.

The Gata2-SNAP allele is a valuable new tool, and it would benefit from slightly more quantitative validation in the supplement. A brief characterization of basic hematopoietic parameters in homozygotes (CBC, LSK/HSPC frequencies, or colony assays) would confirm that the tagged allele is truly physiological and would serve the community that will want to

use this mouse going forward. If this has been done, please include it; if not, a statement about what was checked would suffice.

https://doi.org/10.7554/eLife.111233.1.sa1

Author response:

We are writing to provide our provisional response to the public reviews. We note that the reviewers' comments focus primarily on strengthening technical rigor and quantitative interpretation. We have designed the planned revisions to directly address the reviewers' major concerns and to strengthen the study's evidentiary basis. We plan to submit a revised manuscript for the final Version of Record.

For clarity, we summarize below the major new experiments and analyses that address the reviewers' primary concerns:

(1)Validation of Tracking Parameters (Reviewers 1 & 3): We will re-analyze our single molecule tracking data with tighter gap-time allowances (0 seconds) to demonstrate the robustness of our interpretations of short- and long-lived kinetics. We will also generate a supplementary movie with binding trajectories superimposed directly on detected molecules to visually confirm tracking robustness.

(2) Photobleaching & Two-State Controls (Reviewers 1 & 3): We will report per-cell photobleaching lifetimes derived from our global fluorescence decay. To strengthen this analysis, we will include supplementary measurements using a H2B-HaloTag control under matched imaging conditions and perform single-molecule tracking of GATA2 zinc-finger deletion mutants (N-terminal, C-terminal, and double) as a binding-deficient functional control.

(3) Protein Expression & Labeling Efficiency (Reviewers 1 & 2): To address concerns about transgene expression and competition with endogenous proteins, we will quantify Halo-GATA2 levels in G1E-ER4 and HPC7 cells and SNAP-GATA2 levels in primary cells using standardized titration methods with established Halo-CTCF and SNAP-RPB1 reference systems.

(4) Integration of SMT and CUT&Tag (Reviewer 3): We have conducted a quantitative foldchange analysis of our existing CUT&Tag dataset to complement our single-molecule kinetics.

However, as detailed in our specific response below (R3 point 5), we emphasize that directly integrating population-level genomic occupancy measurements with single-cell kinetic measurements is not straightforward. We will therefore frame the relationship between these datasets as a conceptual consistency check rather than a strict quantitative integration. This quantitative analysis supports and refines the Early-restricted peak set, identifying a high confidence strict subset consistent with the broader presence/absence-defined set described in Figure 5 of the manuscript (see Author response images 1–3 and our response to R3 point 7).

(5) Characterization of the GATA2-SNAP Mouse (Reviewer 3): We have characterized hematopoietic populations in the homozygous knock-in mouse, including lymphoid ($CD3^+/CD4^+/CD8^+/B220^+/CD19^+$), myeloid ($CD11b^+/Gr1^+$), and erythroid ($Ter119^+$) compartments. These data, presented in Author response image 4, indicate that normal mature hematopoietic output is preserved across genotypes. Statistical caveats are described in the corresponding figure legend and in our response to R3 point 8.

> ***Public Reviews:***

> ***Reviewer 1 (Public review):***
>
> *(1) Two binding states: justification and controls*
>
> *The authors propose two states of GATA2 binding. Are there only two states? Some longbinding duration distributions here are very long-tailed (e.g., Figure 2D middle), suggesting a possible third state. The authors must explain how they determined that two states provide the best fit and how they classified short versus long binding. Controls should be included for long-lived and short-lived binding (e.g., histone proteins, HaloTag-NLS, or a binding-deficient GATA2 mutant).*

Agreed in part; we will attempt the requested binding-deficient control using existing GATA2 deletion constructs, complemented by GRID and H2B-HaloTag controls.

We will clarify that the two-state framework is an operational model rather than a claim that GATA2 can occupy only two physical states. This approach is widely used in SMT studies of chromatin-associated transcription factors and transcription machinery (Gebhardt et al., 2013; Liu et al., 2014; Hansen et al., 2017; Kenworthy et al., 2022). In particular, Ling et al. (Science, 2026) recently used two-exponential survival-probability fitting across 58 Halotagged transcription-associated proteins to distinguish transient and stable chromatin-binding populations, while explicitly noting that the simplified two-state model provides a tractable framework even when the underlying physical behavior may be more heterogeneous.

We agree that our current two-state model may under-represent the diversity of GATA2 chromatin-binding populations in single cells. However, even within this simplified framework, the existing analysis already indicates increased upper-tail dispersion of kinetic measurements (e.g., residence time and/or percentage of stable events) at the single-cell level in early erythroid cells. To support the goodness-of-fit metrics from our two-state fitting, as Reviewer 3 recommends, we will provide a supplementary table containing confidence intervals for the rate parameters and an F-test metric describing the differences between one- and two-state fits.

To determine whether additional binding states exist, we will perform GRID (Genuine Rate Identification from Distributions), which does not bias the model toward a particular number of states and, in our experience across multiple proteins, yields fits with 3-5 binding populations. However, we have found that in many cases, GRID requires aggregating binding events from multiple cells to achieve consistently robust fits for the populations of relatively rare, long-lived (>~30 sec) binding events. Therefore, GRID will assess whether additional populations exist, but we will lose the ability to analyze changes in the cell populations at the single-cell level.

We will include the multi-state analysis as a new supplementary figure. We will additionally clarify in the Results and Methods exactly how short- and long-lived binding events are classified (1-second threshold consistent with prior single-molecule frameworks for transcription-factor chromatin interactions; Gebhardt et al., 2013; Liu et al., 2014; Kenworthy et al., 2022) and direct the reviewer to these passages.

For the requested controls, we will include H2B-HaloTag imaging under matched conditions as a long-lived reference for both photobleaching correction and as a positive control for stable chromatin association, addressing R1 point 2 and R3 point 1 simultaneously.

We will also attempt to address the reviewer's request for a binding-deficient control. We have lentiviral constructs in hand that encode GATA2 with a C-terminal zinc-finger deletion (which removes the primary DNA-binding domain), an N-terminal zinc-finger deletion, and a double deletion. We will perform single-molecule tracking of these mutants in the engineered

cell systems and test whether removing GATA2's specific DNA-binding capacity produces the predicted reduction in long-lived chromatin engagement, providing a functional perturbation control. The interpretation of these experiments will depend on the mutants expressing and localizing appropriately, which we will validate before drawing kinetic conclusions. We note that an analogous binding-deficient mutant cannot be examined in the physiological context of the Gata2SNAP knock-in mouse, and we will frame the cell-line mutant analyses accordingly. Together with GRID and the H2B-HaloTag control, these mutants provide complementary lines of validation for the two-state kinetic framework.

> *(2) Photophysical and focal-plane artifacts*
>
> *The authors should exclude contributions from (i) photobleaching, (ii) blinking, and (iii) Z-axis motion. Describe and quantify the photobleaching correction. Provide analyses or controls that distinguish true dissociation events from photophysical blinking/bleaching or axial motion.*

Agreed.

We will substantially expand the methodological description and provide three new pieces of supplementary analysis:

- Photobleaching: A per-cell photobleaching-rate distribution will be plotted for each cell type and differentiation stage, and photobleach-corrected residence-time values will be reported alongside apparent values in the relevant figures. We will also perform H2B-HaloTag imaging under matched illumination, exposure, and dye conditions in each cell line as a longlived chromatin-bound reference, establishing per-cell-type bleach lifetimes to which the GATA2 measurements can be referenced. This approach follows recent SMT precedent in which H2B decay was used to correct residence-time measurements for photobleaching, chromatin and nuclear motion, microscope drift, defocalization, and dye photophysics (Ling et al., Science 2026). The right-censoring photobleach-correction model used in our analysis will be described in detail in the revised Methods, including parameter values and per-cell handling.

- Blinking: The STRAP single-particle tracking pipeline already accommodates fluorophore blinking when linking trajectories across successive frames, following the multiple-targettracing framework of Sergé et al. (Nature Methods, 2008). This use of short gap-frame allowances to avoid artificially splitting trajectories due to fluorophore blinking or transient defocalization is consistent with recent live-cell SMT studies of chromatin-associated factors (Ling et al., Science 2026). We will add an explicit statement to the Methods describing how blinking-tolerant linkage parameters are set, and we will reanalyze representative datasets

with stricter maximum off-frame settings to ensure this parameter does not drive our conclusions (also addressing R3 point 6).

- Z-axis motion: Given our 500-ms exposure and the ~500-nm axial detection range of the HiLo configuration, axial loss is expected to be a minor contributor. We will quantify this indirectly by plotting, as a supplementary analysis, the maximum in-plane 2D spatial exploration of each binding trajectory, defined as the long-axis diameter of the 2D trajectory envelope. Although this does not directly measure z-position, it serves as a control for large apparent displacements that could reflect molecules moving out of the HiLo detection volume and demonstrates that observed dissociation events are not dominated by axial drift.

Representative photobleaching traces from individual cells (lowest, highest, and median bleach rates) will be included to support the single-molecule interpretation (also addresses R1 point 5).

> *(3) HILO illumination and nuclear region sampled*

> *HiLo is sensitive to illumination angle: slight changes sample different nuclear regions. Explain how the HiLo angle was controlled and confirmed comparable across cells and conditions.*

Agreed.

We will add a Methods subsection describing our HiLo illumination procedure. In brief, we started at a TIRF-supercritical angle and reduced it toward epifluorescence just enough to achieve high imaging depth while minimizing out-of-focus background signal. Within each biological system (cell line or primary cells), the TIRF angle was held constant across Basal, Early, and Late conditions to ensure direct comparability of kinetic measurements across stages.

> *(4) Quantification of event counts and long-binding durations*
>
> *The number of binding events and the duration of long-binding events are influenced by imaging conditions. Provide a more detailed analysis of how these variables were controlled and assess the sensitivity of the results to detection and tracking parameters.*

Agreed.

We will (i) normalize per-cell binding-event counts to nuclear cross-sectional area (extracted from the segmented nuclear masks already in the STRAP pipeline) to control for differences in nuclear size; (ii) report the tracking-parameter sensitivity sweep described above; and (iii) confirm in the revised Methods that all imaging conditions (laser power, exposure, dye concentration, sample preparation) were held constant across stages and cell types, consistent with the existing manuscript text. Per the Reviewing Editor's guidance, the planned labeling-efficiency and absolute-molecule-quantification experiments will further constrain the interpretation of binding-event counts across conditions.

> *(5) Evidence that spots are single molecules*
>
> *Provide evidence that spots represent single molecules.*

Agreed.

We will include a small number of per-event intensity traces from our STRAP tracking output, selected to illustrate the single-step photobleaching behavior characteristic of single-molecule emission (intensity remains approximately constant during the binding event and then drops to background in a single step). The nuclear-fluorescence measurements from the planned labeling-titration experiment will also allow us to confirm that bound-spot densities are consistent with single-molecule occupancy at the labeled fraction used for tracking.

> *(6) Description of the spot-analysis pipeline*
>
> *The Methods should include a detailed STRAP pipeline description.*

Partially agreed; the existing STRAP reference is appropriate, but the Methods will be expanded.

STRAP (Haque & Coleman, 2025) is a consolidated, automated implementation of two well-established, previously published frameworks: SLIMfast / multipletarget tracing (Sergé et al., 2008) and evalSPT (Normanno et al., 2015), both of which are cited in the original manuscript. We will expand the Methods to describe the parameter set used in our analysis (detection thresholds, linking radii, gap-frame allowance, photobleaching correction model) so that readers can assess the analysis without referring exclusively to the STRAP manuscript and code repository, while preserving the cited STRAP reference for the full algorithmic

description. We respectfully suggest that a complete pipeline description duplicating Haque & Coleman (2025) would not be appropriate in a primary research article.

> *(7) Differences among cell systems*
>
> *The three cell systems yield notably different results. Provide a more detailed explanation for these differences.*

Agreed.

We will also explicitly describe the caveats of the engineered systems versus the native GATA2-SNAP primary-cell system, in which endogenous GATA2-SNAP remains under physiological regulation. Specifically, we will discuss how variables such as the GATA1null background, ectopic forced nuclear import of GATA1-ERT, and ectopic GATA2-Halo in G1E-ER4 cells, as well as ectopic GATA2-Halo, endogenous GATA1, and cytokine signaling in HPC7 cells, likely contribute to the observed differences in signatures.

> ***Reviewer 2 (Public review):***
>
> *(1) Expression levels of the GATA2-HaloTag transgene*
>
> *Determine the expression levels of the GATA2-HaloTag transgene over the course of differentiation under the conditions used for single-molecule imaging.*

Agreed.

This is the central concern flagged by the Reviewing Editor. For each cell line (G1E-ER4 and HPC7), we will (i) measure total nuclear GATA2-Halo fluorescence per cell under matched acquisition conditions and (ii) convert this fluorescence intensity to absolute molecules per cell using a Halo-CTCF/U2OS reference standard (Cattoglio et al., 2019; absolute CTCF abundance quantification applied previously by our group). This will provide per-cell GATA2Halo molecule counts at each differentiation stage (Basal, Early, Late). For the primary GATA2SNAP cells, we will perform the analogous comparison against a SNAP-RPB1/U2OS standard.

> *(2) Fraction of molecules labeled*
>
> *Carry out a titration of the HaloTag ligand and compare the amount of labeled protein under single-molecule imaging conditions to that of saturating labeling.*

Agreed.

We will perform HaloTag-ligand and SNAP-tag-ligand titrations in each cell type, comparing nuclear fluorescence under the limiting-label conditions used for single-molecule tracking with that under saturating labeling. This will yield a per-cell-type labeled fraction and allow us to confirm that comparisons of binding-event counts across conditions are not confounded by differences in labeling efficiency. The labeled-fraction values will be reported in a new supplementary figure and incorporated into our quantification of binding-event rates.

> *(3) Robust single-particle tracking*
>
> *Show images of particle trajectories or movies superimposing trajectories on imaging data.*

Agreed.

We will generate visualizations of selected long-lived binding events with single-particle trajectories overlaid on the imaging data — using a multi-frame color overlay (e.g., five sequential frames in distinct colors superimposed) so that linkage of the spot across frames is

visually unambiguous — and include them as a new supplementary figure or movie. Examples will be drawn from each cell system to demonstrate consistent tracking quality.

> ***Reviewer 3 (Public review):***
>
> *(1) Photobleaching correction; per-cell bleach lifetimes*
>
> *Report the per-stage (or per-cell) photobleaching lifetimes and the photobleachcorrected residence time values alongside apparent values, ideally with an H2B-Halo control.*

Agreed.

Addressed by the photobleach-rate distribution and H2B-HaloTag control analyses described under R1 point 2. The supplementary figure will explicitly compare per-cell bleach lifetimes across stages, report photobleach-corrected residence-time values alongside apparent values and include H2B-HaloTag controls under matched conditions in each cell line.

> *(2) Mechanistic differences across systems*
>
> *The three systems show qualitatively different signatures: residence time change in G1EER4, bound fraction expansion in HPC7 and primary cells. Reporting an on-rate proxy alongside k_off would help.*

Agreed.

Addressed by the cross-system kinetic framing described under R1 point 7 and by the GRID state-spectrum analysis described under R1 point 1. We will explicitly frame the three systems in terms of underlying kinetic mechanism in both Results and Discussion, following the conceptual distinction emphasized by Ling et al. (Science 2026) in which residence time reports binding stability once engaged, whereas changes in bound fraction or event frequency can indicate altered association/recruitment efficiency. In this framework, the G1E-ER4 residencetime signature is consistent with reduced dissociation (a longer-lived bound state), while the longlived-fraction expansion in HPC7 and primary cells is consistent with an increased target-search efficiency or specific-binding-competent pool. Alongside the GRID-derived state-spectrum analysis, we will report an apparent engagement-rate proxy calculated as binding events per unit imaging time normalized to detectable molecule number; this proxy is an approximation, not a direct k_on measurement, as accurate determination of k_on from single-molecule tracking requires concentration-dependent on-rate experiments that are outside the scope of the present study. We thank the reviewer for this suggestion, which we agree sharpens rather than alters the central message.

> *(3) Per-cell GATA2 concentration and the uncoupling claim*
>
> *Quantify total nuclear GATA2-Halo signal per cell across stages; for primary cells, a western blot or quantitative immunofluorescence on flow-sorted populations would make the uncoupling argument more defensible.*

Agreed.

For the cell lines, the per-cell nuclear GATA2-Halo quantification described in our response to R2 point 1 addresses this point.

For primary cells, where the biological claim is strongest, we will exploit the endogenous Gata2SNAP knock-in itself as a quantitative reporter of total GATA2 protein. Specifically, we will label flow-sorted CD71/Ter119 populations from Gata2-SNAP mouse bone marrow with SNAP-Cell 647-SiR at saturating concentration in a parallel acquisition to the limiting-label single-molecule tracking experiment. Total nuclear SNAP-GATA2 fluorescence at saturating labeling provides a measure of endogenous GATA2 abundance per cell at each erythroid

stage, in the same chemistry used for our single-molecule measurements, and will be benchmarked against a SNAPRPB1/U2OS reference standard for absolute molecule counting. This approach (i) measures the protein of interest in the labeling chemistry already established in this study; (ii) avoids reliance on quantitative immunofluorescence, which we have not been able to validate under our flowsorted-cell conditions; and (iii) extends the same analytical framework — saturating versus limiting labeling, with U2OS reference standards — across cell lines and primary cells. Quantitative western blotting on flow-sorted populations remains an alternative we will consider if specifically requested by the reviewers.

> *(4) Single-cell distribution analysis*
>
> *Distribution-based statistics (K-S test, mixture model) rather than (or alongside) meanbased ANOVA, particularly for the Early populations, which look potentially bimodal.*

Agreed.

We will perform Kolmogorov–Smirnov and Gaussian mixture model analyses of the single-cell long-lived fraction and residence-time distributions across stages, reporting these alongside the existing Welch ANOVA results in a new supplementary figure. This analysis is consistent with the conceptual framework cited in the manuscript (Wheat et al., 2020; Palii et al., 2019) for probabilistic hematopoietic transitions and may reveal subpopulation structure underlying the Early-stage signal. The GRID analysis further complements this by formally testing whether multi-state mixture models are statistically preferred at each stage. However, GRID analysis requires aggregating binding events across cells, which limits our ability to monitor changes in population dispersion at the single-cell level.

> *(5) Quantitative integration of CUT&Tag with SMT*
>
> *Attempt a back-of-the-envelope calculation of whether the residence-time or fraction changes are quantitatively consistent with the acquisition of the 1,167 Early-restricted sites.*

Partially agreed; will attempt an order-of-magnitude framing.

We thank the reviewer for this thoughtful suggestion. We agree that more explicit framing of the quantitative relationship between the two datasets will strengthen the integration. We will add a paragraph to the Discussion presenting an order-of-magnitude calculation linking the observed residence-time and long-lived-fraction changes to the steady-state occupancy increase predicted at competent regulatory sites, with explicit caveats regarding (i) the inherently semi-quantitative nature of CUT&Tag signal and (ii) the assumptions required to translate population-averaged occupancy into the genome-wide site count observed. For the G1EER4 cells, we observe relatively minor shifts in population-mean behavior as single-cell dispersion increases. Therefore, it may be difficult to directly link population-based measurements (e.g. CUT&Tag) with single-cell kinetic measurements (SPT). This distinction between occupancy and dynamics is consistent with recent systematic SMT analysis of the eukaryotic transcription machinery, in which factors appearing persistently associated in ensemble genomic assays were shown to exchange on second-scale timescales in living cells (Ling et al., Science 2026), emphasizing that population genomic occupancy and single-molecule residence time are complementary but not directly interchangeable measurements. Closing this gap rigorously is a major hurdle for the field and will require substantial technology development on quantitative single-cell CUT&Tag occupancy measurements. We will therefore frame our analysis as a consistency check rather than a strict quantitative integration. The reviewer notes that this analysis “does not change the central message; it sharpens it,” and we agree.

> *(6) Short-lived kinetic interpretation and tracking parameters*
>
> *The 1.5 s gap allowance is long relative to the short-lived residence times in primary cells. A sensitivity analysis with tighter gap parameters would help. Also clarify how slowing of search reconciles with increased binding events at Early.*

Agreed.

Addressed by the tracking-parameter sensitivity analysis described under R1 point 2. We apologize for the lack of clarity in our original description of the gap allowance. Our current maximum off-frame parameter is set to 2 frames, corresponding to a 0.5-s gap allowance. We will rerun the tracking analysis on representative datasets using a maximum off-frame parameter of 1, corresponding to no missed frames, and will report the resulting residence-time distributions alongside the original analysis to demonstrate robustness. We will also clarify in the Results and Discussion how changes in short-lived binding kinetics are reconciled with the increase in detectable binding events at the Early stage, drawing on the apparent engagement-rate proxy interpreted alongside the GRID-derived state-spectrum analysis.

> *(7) CUT&Tag peak definition and quantitative analysis*
>
> *Report (a) signal intensity distribution at the 1,167 sites across stages (scatter or density plot beyond the heatmap) or (b) differential binding analysis (e.g., DESeq2). State replicate count and overlap of Early-restricted sets across replicates.*

Agreed; normalized fold-change analysis completed, with replicate-aware differential binding analysis planned if additional replicates are generated.

We have performed a normalized count-based fold-change analysis of the union peak set from the existing GATA2 CUT&Tag dataset (14,468 peaks) using the goodpeaks framework previously used in our group, yielding per-peak log2 fold-change values and discrete dynamicstatus calls (Gained / Lost / Unchanged at $|\log2FC| \geq 2$) for each of the two transitions (Basal → Early at 0 vs 2 h, and Early → Late at 2 vs 24 h). This provides a conservative quantitative complement to the presence/absence peak-calling analysis presented in Figure 5; if additional replicate data are generated, we will perform replicate-aware differential binding analysis (DiffBind/DESeq2; Love et al., 2014; Stark & Brown, 2011) and report replicate overlap. This analysis addresses option (b) of the reviewer's request and also enables the visualization requested in option (a) as a cross-stage scatter (Author response image 1). We present the quantitative analysis as a supplement to the presence/absence-defined Early-restricted set in Figure 5 of the manuscript, providing two orthogonal lines of evidence for the same biology. We note that the CUT&Tag experiments were initially performed as a validation step to confirm that the tagged GATA2-Halo constructs recapitulate endogenous chromatin-binding behavior, including appropriate genomic localization and expected GATA switch dynamics. This validation supports the conclusion that the observed single-molecule kinetics reflect physiologically relevant GATA2 engagement. Having established this, we subsequently extended the dataset to perform the quantitative analyses presented here.

Quantitative findings.

- 384 peaks were Gained ($|\log2FC| \geq 2$) at the Basal → Early transition.

- 1,006 peaks were Lost over the same transition.

- 178 peaks were Gained at Basal → Early and subsequently Lost at Early → Late, defining the strict differentially-restricted Early set (Author response image 1, red points). This set represents the higher-confidence subset of the manuscript's broader presence/absence-

defined Earlyrestricted set (n = 1,167; defined as MACS2 peaks at q < 0.01 present at Early but absent at Basal and Late).

- 200 peaks were Gained at Early and retained at Late, indicating stable acquisition.

- 49 peaks were acquired only at the Late stage.

The discrepancy between the broader presence/absence set (1,167) and the strict differential set (178) reflects the analytical choice the reviewer raised: presence/absence calls based on a peaksignificance threshold are sensitive to near-threshold peaks, whereas differential analysis with a fold-change cutoff captures only sites with quantitatively pronounced stage-restricted enrichment. We interpret these as two complementary definitions: the broader set captures all peaks meeting a stage-specific peak-calling criterion, and the strict subset isolates the most quantitatively dynamic core of that population.

Importantly, the three named example loci shown in Figure 5D of the manuscript — Nono (promoter-proximal), Nr3c1 (intron 2), and Gata3 (distal intergenic) — all survive the strict differential criterion (each shows $|\log^{2FC}| \geq 2$ in both transitions, consistent with a clean Gainedthen-Lost signature). The published example panel therefore represents the high-confidence intersection of both definitions, supporting the robustness of the manuscript's selected illustrative cases.

We will explicitly state the number of CUT&Tag replicates per stage in the revised Methods and figure legends. Where the differential analysis is currently based on a single replicate per stage, we will explicitly note this and treat the strict subset as a conservative confirmatory analysis. An additional replicate is under consideration for the full revision, and if performed, overlap of Earlyrestricted calls across replicates will be reported.

Motif cross-validation against a matched-GC background using HOMER and/or MEME-ChIP is planned for the strict differential subset and will be reported alongside the original SeqPos analysis in the revised Figure 5F or its supplement.

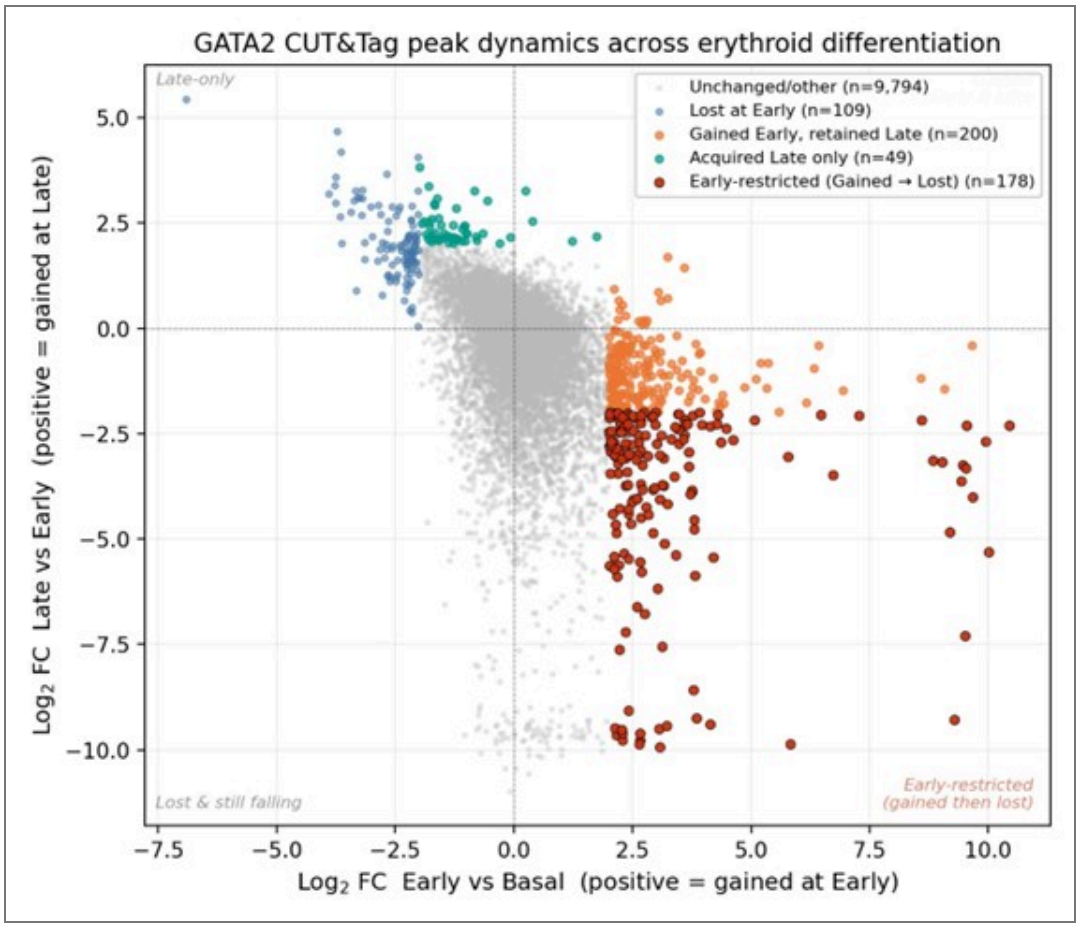

Author response image 1. Cross-stage log_2 fold-change scatter for GATA2 CUT&Tag peaks. Each point represents a single peak in the union peak set (n = 14,468). The x-axis shows the log2 fold change from Basal (0 h) to Early (2 h); the y-axis shows the log2 fold change from Early (2 h) to Late (24 h). The sign convention follows the field-standard direction (positive log2FC = increased signal at the later time point). Peaks are colored by dynamic-status classification: unchanged/other (gray; n = 9,794); Lost at Early (blue; n = 109); Gained at Early and retained at Late (orange; n = 200); acquired only at Late (teal; n = 49); and Early-restricted, defined as Gained at Early and Lost at Late with |log2FC| ≥ 2 in both transitions (red; n = 178). The Early-restricted population occupies the lower-right quadrant, consistent with a transient kinetic peak of GATA2 binding.

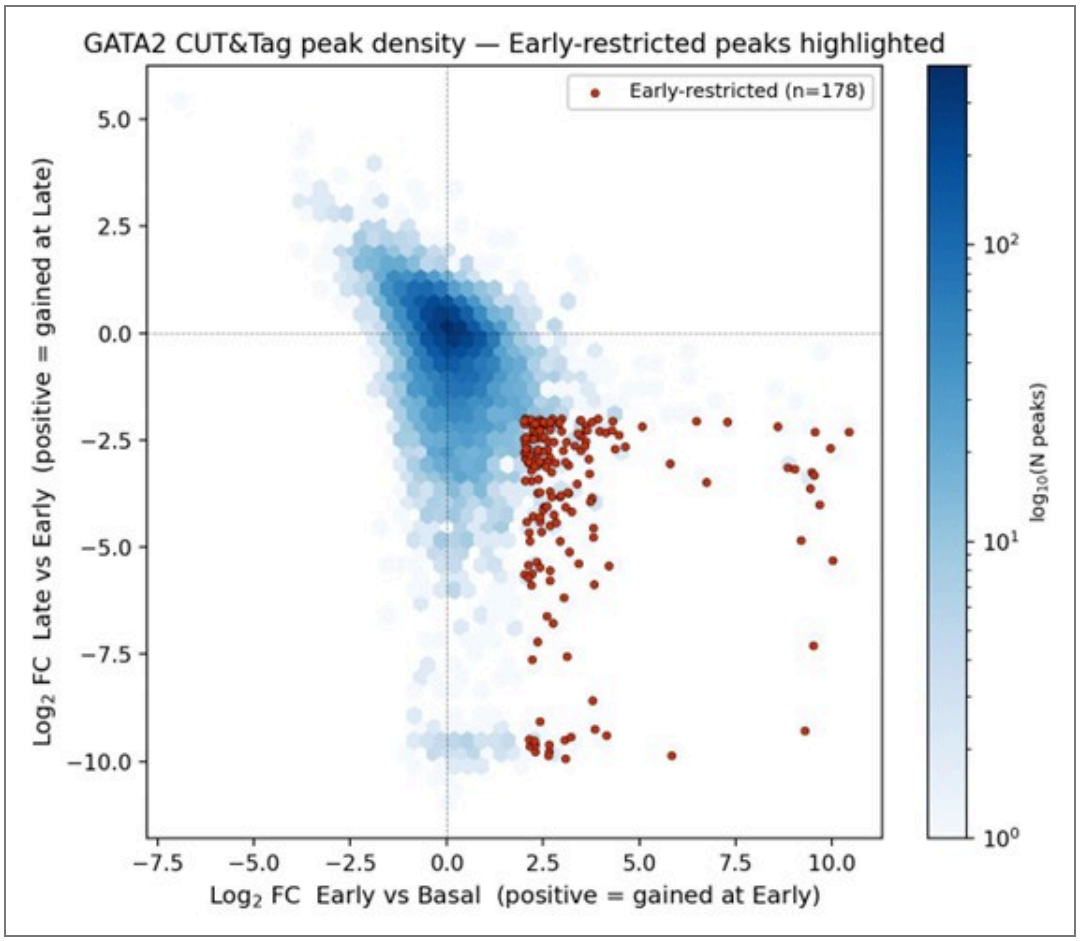

Author response image 2. Density representation of GATA2 CUT&Tag peak dynamics with Early-restricted peaks highlighted.

Author response image 2 is shown for illustrative reference and is not annotated with a separate legend; it presents the same data as Author response image 1 in a hexbin density format to emphasize the bulk of unchanged peaks at the origin and the spatial separation of the Early-restricted set.

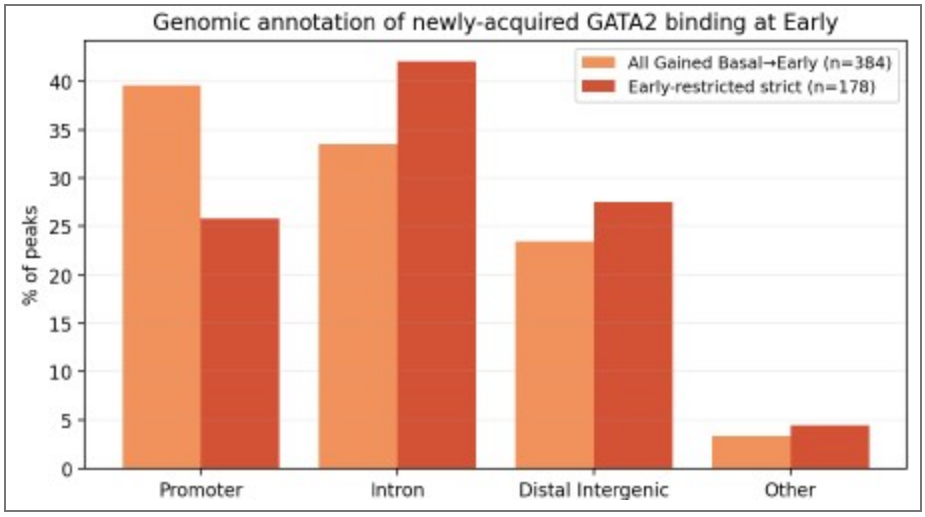

Author response image 3. Genomic-annotation comparison of newly acquired GATA2 binding at Early. Stacked-bar comparison of genomic annotations (ChIPseeker classification) for two definitions of the newly acquired GATA2 peaks at the Early erythroid stage: all peaks Gained at Basal → Early (orange; n = 384) and the

strict Early-restricted subset (Gained then Lost; red; n = 178). Annotation categories shown: Promoter (≤1 kb of TSS), Intron, Distal Intergenic, and Other (Exon, 5'/3' UTR, Downstream). Both peak sets contain substantial promoter-proximal and distal/intronic components, consistent with the two-subclass model described in Figure 5E–G of the manuscript (GATA2-only promoter-proximal peaks with GATA/RUNX motifs, and GATA2/GATA1 cobound distal peaks with composite GATA/E-box motifs). The strict subset shows a higher proportion of intronic and distal-intergenic sites and a lower proportion of promoter-proximal sites than the full Gained set; this difference will be discussed transparently in the revised Results. Motif analysis (HOMER/MEME-ChIP, planned for the full revision) will be performed on both peak sets to confirm that the GATA/RUNX and GATA/E-box subclass signatures are preserved.

> *(8) Knock-in mouse hematopoietic validation*
>
> *A brief characterization of basic hematopoietic parameters in homozygotes (CBC, LSK/HSPC frequencies, or colony assays) would confirm the tagged allele is physiological.*

Agreed; data acquired and analyzed.

We have characterized mature trilineage hematopoietic populations in whole bone marrow from wild-type, heterozygous (Gata2Het), and homozygous (Gata2Homo) Gata2-SNAP knock-in mice (n = 5 per genotype). Bone marrow cells were stained for myeloid ($CD11b^+$ $Gr1^+$), lymphoid ($CD3^+$/$CD4^+$/$CD8^+$/$B220^+$/$CD19^+$), and erythroid ($Ter119^+$) markers and analyzed by flow cytometry. Lineage frequencies are shown as percentages of live bone marrow cells in a new Figure Supplement in the revised manuscript.

For myeloid and erythroid populations, omnibus one-way ANOVA detected no significant differences across genotypes (Myeloid: $F(2,12) = 2.616$, $P = 0.1140$; Erythroid: $F(2,12) = 0.4943$, $P = 0.6219$). Dunnett's multiple-comparisons test against the WT control did not detect significant pairwise differences for either knock-in genotype (Myeloid: WT vs Het $P = 0.1351$, WT vs Homo $P = 0.9926$; Erythroid: WT vs Het $P = 0.7017$, WT vs Homo $P = 0.9602$).

For the lymphoid compartment, although the omnibus ANOVA reached significance ($F(2,12) = 6.690$, $P = 0.0112$), no pairwise comparison against WT remained significant after multiplecomparisons correction (Dunnett's adjusted P values: WT vs Het = 0.1217; WT vs Homo = 0.2078). We therefore interpret this result conservatively. Brown-Forsythe and Bartlett's tests showed no significant differences in variance across genotypes ($P = 0.1423$ and $P = 0.0908$), so the result is not attributable to unequal variances. We do not interpret these data as indicating an unambiguous lymphoid phenotype in either heterozygous or homozygous Gata2-SNAP mice; this interpretation is consistent with the broader pattern across all three lineages, in which no pairwise comparison against WT survives multiple-comparisons correction. We will note in the figure legend and in the Results text that more granular HSPC-compartment analysis (LSK, MPP, lineage-restricted progenitor frequencies) and a complete blood count (CBC) remain valuable directions for future characterization of this resource and will be considered for the full revision if specifically requested.

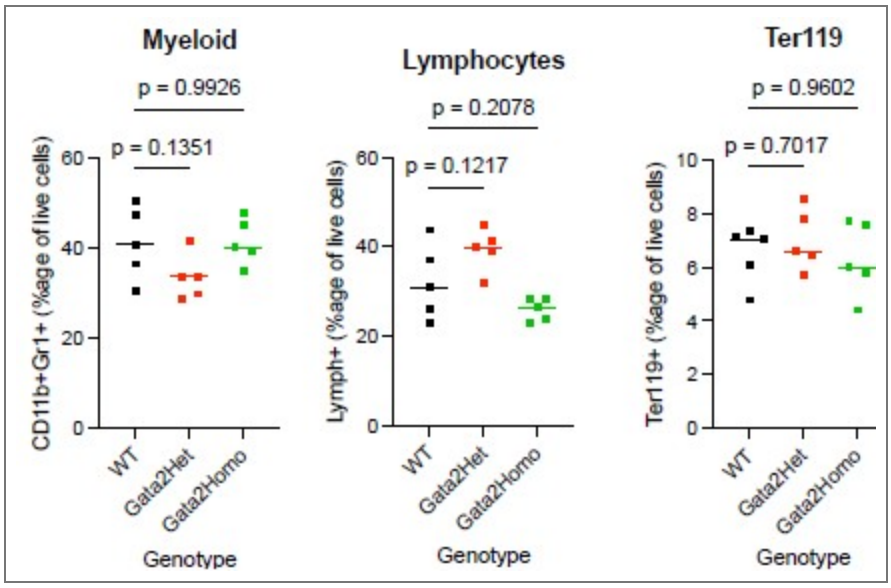

Author response image 4. Bone marrow trilineage frequencies in Gata2-SNAP knock-in mice. Bone marrow was harvested from the femurs and tibias of wild-type (WT), heterozygous (Gata2Het), and homozygous (Gata2Homo) Gata2-SNAP knock-in mice (n = 5 per genotype; mixed sex; 12–14 weeks). After ACK lysis, cells were stained for myeloid ($CD11b^+$ $Gr1^+$), lymphoid ($CD3^+/CD4^+/CD8^+/B220^+/CD19^+$), and erythroid ($Ter119^+$) markers and analyzed by flow cytometry. Each dot represents one mouse, and horizontal bars indicate genotype means. Statistical results: Myeloid: ANOVA F(2,12) = 2.616, P = 0.1140; Dunnett's adjusted P values WT vs Het = 0.1351, WT vs Homo = 0.9926. Lymphoid: ANOVA F(2,12) = 6.690, P = 0.0112 (omnibus); Dunnett's adjusted P values WT vs Het = 0.1217, WT vs Homo = 0.2078. Erythroid: ANOVA F(2,12) = 0.4943, P = 0.6219; Dunnett's adjusted P values WT vs Het = 0.7017, WT vs Homo = 0.9602. Brown-Forsythe and Bartlett's tests for unequal variance were non-significant in all three lineages. Although the lymphoid omnibus ANOVA reached nominal significance, no pairwise comparison with WT remained significant after multiple-comparison correction; we therefore interpret this result conservatively (see response to R3 point 8).

Summary

We thank the editors and the three reviewers for the constructive and detailed assessment. The planned revisions consist of:

- Four new experiments [planned] (HaloTag/SNAP labeling efficiency and absolute molecule counts via U2OS reference standards; H2B-HaloTag photobleaching reference; percell quantification of total endogenous GATA2 in flow-sorted primary Gata2-SNAP populations via saturating SNAP-tag labeling, benchmarked against a SNAP-RPB1/U2OS reference standard; single-molecule tracking of GATA2 N-terminal, C-terminal, and double zinc-finger deletion mutants in the engineered cell systems as a binding-deficient functional control).

- Six analyses of existing data (GRID multi-state fitting [planned]; per-cell bleach-rate distributions and photobleach-corrected residence times [planned]; tracking-parameter sensitivity [planned]; nuclear-area normalization and total-displacement controls [planned]; normalized fold-change CUT&Tag analysis [completed; motif cross-validation planned], presented in Author response images 1–3; distribution-based single-cell statistics [planned]).

- One previously-acquired dataset [completed] (trilineage hematopoietic flow cytometry of homozygous Gata2-SNAP knock-in mice; presented in Author response image 4 with full statistical detail).

- Substantial revisions to text and figures [planned] to address statistical reporting, methodological description, mechanistic framing of cross-system differences, and refinement of the Figure 6 schematic.

With respect to the requested binding-deficient single-molecule control, we will attempt to address this directly using sequence-validated lentiviral constructs in hand encoding GATA2

mutants lacking the C-terminal zinc finger, the N-terminal zinc finger, or both. These mutant analyses will be complemented by GRID multi-state analysis and H2B-HaloTag controls, providing converging lines of validation for the two-state kinetic framework. We note that an analogous mutant cannot be examined in the physiological context of the Gata2-SNAP knock-in mouse, and we will frame the cell-line mutant analyses accordingly.

We believe these revisions directly address the editors' specific guidance regarding labeling efficiency and methodological clarification. We thank the editors and reviewers for their time and look forward to submitting the revised manuscript.

References cited in this response:

References listed below are cited in this provisional response in support of the planned analyses and methodology.

Cattoglio, C., Pustova, I., Walther, N., Ho, J. J., Hantsche-Grininger, M., Inouye, C. J., Hossain, M. J., Dailey, G. M., Ellenberg, J., Darzacq, X., Tjian, R., & Hansen, A. S. (2019). Determining cellular CTCF and cohesin abundances to constrain 3D genome models. eLife, 8, e40164. *https://doi.org/10.7554/eLife.40164*

Gebhardt, J. C. M., Suter, D. M., Roy, R., Zhao, Z. W., Chapman, A. R., Basu, S., Maniatis, T., & Xie, X. S. (2013). Single-molecule imaging of transcription factor binding to DNA in live mammalian cells. Nature Methods, 10(5), 421–426. *https://doi.org/10.1038/nmeth.2411*

Hansen, A. S., Pustova, I., Cattoglio, C., Tjian, R., & Darzacq, X. (2017). CTCF and cohesin regulate chromatin loop stability with distinct dynamics. eLife, 6, e25776. *https://doi.org/10.7554/eLife.25776*

Haque, N., & Coleman, R. A. (2025). Dynamic transcription pre-initiation complex assembly governs initiation efficiency. bioRxiv. *https://doi.org/10.1101/2025.05.07.652662*

Heinz, S., Benner, C., Spann, N., Bertolino, E., Lin, Y. C., Laslo, P., Cheng, J. X., Murre, C., Singh, H., & Glass, C. K. (2010). Simple combinations of lineage-determining transcription factors prime cis-regulatory elements required for macrophage and B cell identities. Molecular Cell, 38(4), 576–589. *https://doi.org/10.1016/j.molcel.2010.05.004*

Kaya-Okur, H. S., Wu, S. J., Codomo, C. A., Pledger, E. S., Bryson, T. D., Henikoff, J. G., Ahmad, K., & Henikoff, S. (2019). CUT&Tag for efficient epigenomic profiling of small samples and single cells. Nature Communications, 10(1), 1930. *https://doi.org/10.1038/s41467-019-09982-5*

Kenworthy, C. A., Haque, N., Liou, S.-H., Chandris, P., Wong, V., Dziuba, P., Lavis, L. D., Liu, W.-L., Singer, R. H., & Coleman, R. A. (2022). Bromodomains regulate dynamic targeting of the PBAF chromatin-remodeling complex to chromatin hubs. Biophysical Journal, 121(9), 1738–1752. *https://doi.org/10.1016/j.bpj.2022.03.027*

Ling, Y. H., Liang, C., Wang, S., & Wu, C. (2026). Live-cell single-molecule dynamics of eukaryotic RNA polymerase machineries. Science, 391, eads0960. *https://doi.org/10.1126/science.ads0960*

Liu, Z., Legant, W. R., Chen, B.-C., Li, L., Grimm, J. B., Lavis, L. D., Betzig, E., & Tjian, R. (2014). 3D imaging of Sox2 enhancer clusters in embryonic stem cells. eLife, 3, e04236. *https://doi.org/10.7554/eLife.04236*

Loeffler, D., Wang, W., Hopf, A., Hilsenbeck, O., Bourgine, P. E., Rudolf, F., Martin, I., & Schroeder, T. (2018). Mouse and human HSPC immobilization in liquid culture by CD43- or CD44-antibody coating. Blood, 131(13), 1425–1429. *https://doi.org/10.1182/blood-2017-07-794131*

Love, M. I., Huber, W., & Anders, S. (2014). Moderated estimation of fold change and dispersion for RNAseq data with DESeq2. Genome Biology, 15(12), 550. *https://doi.org/10.1186/s13059-014-0550-8*

Machanick, P., & Bailey, T. L. (2011). MEME-ChIP: motif analysis of large DNA datasets. Bioinformatics, 27(12), 1696–1697. *https://doi.org/10.1093/bioinformatics/btr189*

Normanno, D., Boudarène, L., Dugast-Darzacq, C., Chen, J., Richter, C., Proux, F., Bénichou, O., Voituriez, R., Darzacq, X., & Dahan, M. (2015). Probing the target search of DNA-binding proteins in mammalian cells using TetR as model searcher. Nature Communications, 6, 7357. *https://doi.org/10.1038/ncomms8357*

Palii, C. G., Cheng, Q., Gillespie, M. A., Shannon, P., Mazurczyk, M., Napolitani, G., Price, N. D., Ranish, J. A., Morrissey, E., Higgs, D. R., & Brand, M. (2019). Single-cell proteomics reveal that quantitative changes in co-expressed lineage-specific transcription factors determine cell fate. Cell Stem Cell, 24(5), 812–825.e5. *https://doi.org/10.1016/j.stem.2019.02.016*

Sergé, A., Bertaux, N., Rigneault, H., & Marguet, D. (2008). Dynamic multiple-target tracing to probe spatiotemporal cartography of cell membranes. Nature Methods, 5(8), 687–694. *https://doi.org/10.1038/nmeth.1233*

Stark, R., & Brown, G. D. (2011). DiffBind: Differential binding analysis of ChIP-Seq peak data. Bioconductor. *http://bioconductor.org/packages/release/bioc/html/DiffBind.html*

Taylor, S. J., Stauber, J., Bohorquez, O., Tatsumi, G., Kumari, R., Chakraborty, J., Bartholdy, B. A., Schwenger, E., Sundaravel, S., Farahat, A. A., Dutta, A., Koche, R. P., Steidl, U., & Wheat, J. C. (2024). Pharmacological restriction of genomic binding sites redirects PU.1 pioneer transcription factor activity. Nature Genetics, 56(10), 2213–2227. *https://doi.org/10.1038/s41588-024-01911-7*

Wheat, J. C., Salsman, J., Reekie, I., Mathhwala, A., Black, K. L., Tiedt, R., Shroff, H., & Steidl, U. (2020). Single-molecule imaging of transcription dynamics in somatic stem cells. Nature, 583(7816), 431– 436. *https://doi.org/10.1038/s41586-020-2432-4*

https://doi.org/10.7554/eLife.111233.1.sa0